



HAL
open science

Delivery of Anticancer Drugs Using Microbubble-Assisted Ultrasound in a 3D Spheroid Model

Marie Roy, Corentin Alix, Julien Burlaud-Gaillard, Damien Fouan, William Raoul, Ayache Bouakaz, Emmanuelle Blanchard, Thierry Lecomte, Marie-Claude Viaud-Massuard, Noboru Sasaki, et al.

► **To cite this version:**

Marie Roy, Corentin Alix, Julien Burlaud-Gaillard, Damien Fouan, William Raoul, et al.. Delivery of Anticancer Drugs Using Microbubble-Assisted Ultrasound in a 3D Spheroid Model. *Molecular Pharmaceutics*, 2024, Online ahead of print. 10.1021/acs.molpharmaceut.3c00921 . inserm-04374054

HAL Id: inserm-04374054

<https://inserm.hal.science/inserm-04374054v1>

Submitted on 5 Jan 2024

HAL is a multi-disciplinary open access archive for the deposit and dissemination of scientific research documents, whether they are published or not. The documents may come from teaching and research institutions in France or abroad, or from public or private research centers.

L'archive ouverte pluridisciplinaire **HAL**, est destinée au dépôt et à la diffusion de documents scientifiques de niveau recherche, publiés ou non, émanant des établissements d'enseignement et de recherche français ou étrangers, des laboratoires publics ou privés.

1 Delivery of Anti-Cancer Drugs using Microbubble- 2 Assisted Ultrasound in a 3D Spheroid Model

3 *Marie Roy¹, Corentin Alix¹, Julien Burlaud-Gaillard², Damien Fouan¹, William Raoul⁴,*
4 *Ayache Bouakaz¹, Emmanuelle Blanchard², Thierry Lecomte^{4,5}, Marie-Claude Viaud-Massuard⁶,*
5 *Noboru Sasaki⁷, Sophie Serrière^{1,3*‡}, Jean-Michel Escoffre^{1*‡}*

6 ¹UMR 1253, iBrain, Université de Tours, Inserm, 37032 Tours, France

7 ²Inserm U1259, Université de Tours et CHRU de Tours & Plateforme IBiSA des Microscopies,
8 PPF ASB, CHRU de Tours, Tours, France

9 ³Département d'Imagerie Préclinique, Plateforme Scientifique et Technique Analyse des
10 Systèmes Biologiques, Université de Tours, 37032 Tours, France

11 ⁴Inserm UMR 1069, Nutrition Croissance et Cancer (N2C), Université de Tours, France

12 ⁵Department of Hepato-Gastroenterology & Digestive Oncology, CHRU de Tours, France

13 ⁶UMR 1100, Centre D'Etude Des Pathologies Respiratoires, Université de Tours, Inserm, Tours,
14 France

15 ⁷Laboratory of Veterinary Internal Medicine, Department of Clinical Sciences; Faculty of
16 Veterinary Medicine, Hokkaido University, Sapporo, Japan

17 RUNNING TITLE

18 Acoustically mediated drug delivery in spheroids

19 AUTHOR INFORMATION

20 *Author contributions*

21 ‡ S.S. and J.M.E. contributed equally to this work. All authors have given approval to the final
22 version of the manuscript.

23 *Corresponding authors*

24 **S. Serrière, Ph.D. and J.M. Escoffre, Ph.D., UMR 1253, iBrain, Université de Tours, Inserm, 10
25 bd Tonnellé, 37032 Tours Cedex 1, France. Tel: +33(0)247366343 (S.S.), Tel: +33(0)247366191
26 (J.M.E.). *Email address:* sophie.serriere@univ-tours.fr and jean-michel.escoffre@univ-tours.fr.

27 *ORCID*

28 Corentin Alix : 0000-0002-1841-0572

29 Julien Burlaud-Gaillard : 0000-0001-5171-9873

30 William Raoul : 0000-0002-5040-3372

31 Emmanuelle Blanchard : 0000-0002-9541-5190

32 Ayache Bouakaz : 0000-0001-5709-7120

33 Thierry Lecomte : 0000-0001-5093-0212

34 Sophie Serrière : 0000-0002-7113-0254

35 Jean-Michel Escoffre : 0000-0003-1041-6950

36 *Notes*

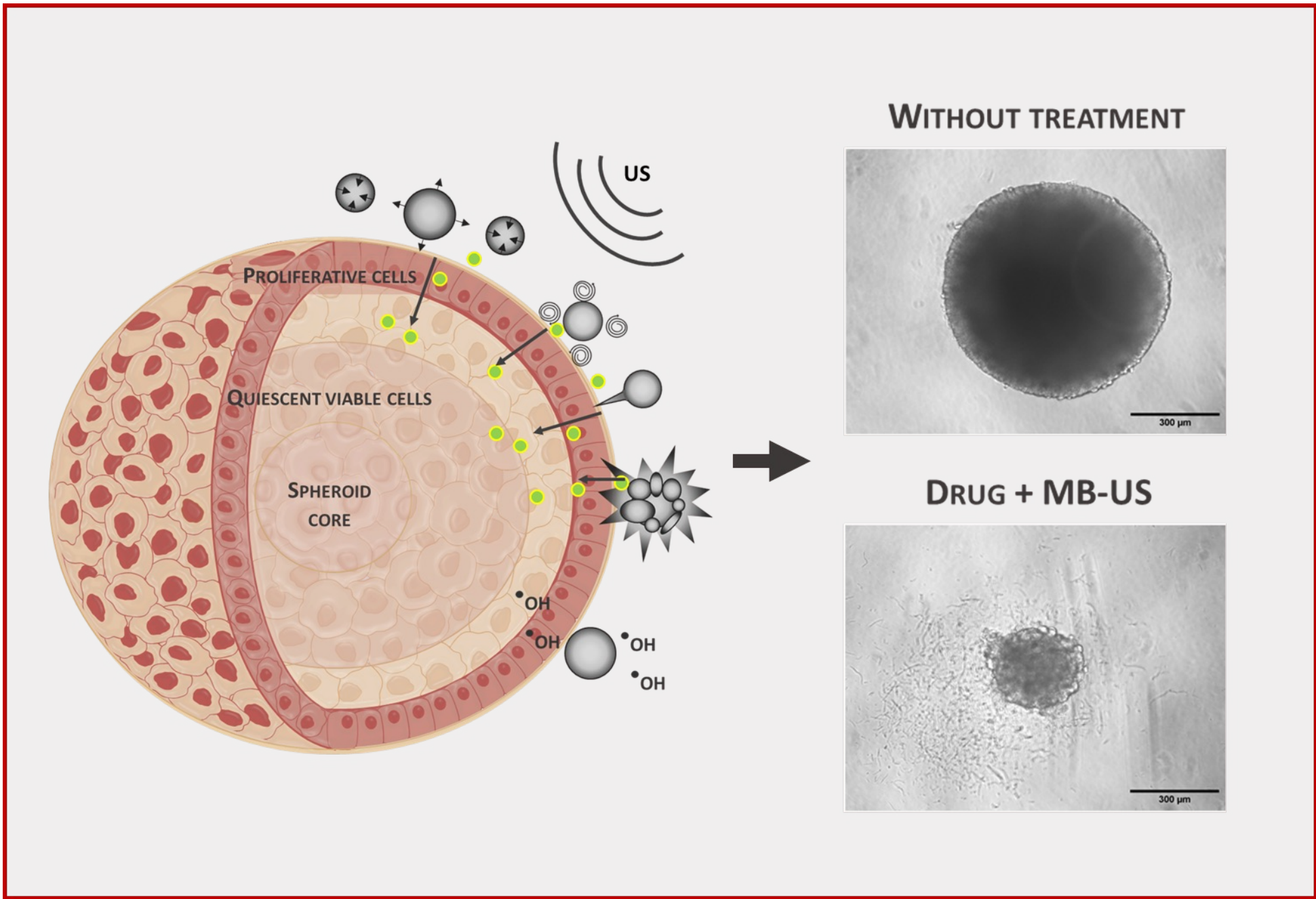
37 The authors declare no competing financial interest.

38 ABSTRACT (200 WORDS)

39 Tumor spheroids are promising 3D *in vitro* tumor models for the evaluation of drug delivery
40 methods. The design of noninvasive and targeted drug methods is required to improve the
41 intratumoral bioavailability of chemotherapeutic drugs and to reduce their adverse off-target
42 effects. Among such methods, microbubble-assisted ultrasound (MB-assisted US) is an innovative
43 modality for noninvasive targeted drug delivery. The aim of the present study is to evaluate the
44 efficacy of this US modality for the delivery of bleomycin, doxorubicin and irinotecan in colorectal
45 cancer (CRC) spheroids. MB-assisted US permeabilized the CRC spheroids to propidium iodide,
46 which was used as a drug model, without affecting their growth and viability. Histological analysis
47 and electron microscopy revealed that MB-assisted US affected only the peripheral layer of CRC
48 spheroids. The acoustically mediated bleomycin delivery induced a significant decrease in CRC
49 spheroid growth in comparison to spheroids treated with bleomycin alone. However, this US
50 modality did not improve the therapeutic efficacy of doxorubicin and irinotecan on CRC spheroids.
51 In conclusion, this study demonstrates that tumor spheroids are a relevant approach to evaluate the
52 efficacy of MB-assisted US for the delivery of chemotherapeutics.

53 KEYWORDS: Microbubble – Ultrasound – Sonoporation – Drug delivery – Spheroid – Colorectal
54 Cancer.

55



Graphical abstract

56 INTRODUCTION

57 Ethical considerations in animal experimentation have led researchers to consider and
58 design new 3D *in vitro* tumor models for drug screening, drug design, drug targeting and drug
59 toxicity, especially when the promising results obtained in 2D *in vitro* tumor models (*e.g.*, cell
60 monolayers, coculture systems, *etc.*) have not been reproduced in animal tumor models. Among
61 these 3D models, tumor spheroids are the most exploited for the design and validation of anticancer
62 strategies. As reported in [1], tumor spheroids are 3D aggregates of tumor cells that may or may
63 not be associated with other cell types, such as fibroblasts or immune cells. These cells interact
64 not only with themselves but also with an extracellular matrix (*i.e.*, endogenous or exogenous),
65 thus creating a dense molecular and cellular network, which limits drug access to tumor cells [2,3].
66 The main physiological consequence of such gradients is the establishment of a peripheral layer
67 of proliferative cells, an intermediate layer of quiescent cells and a necrotic core, as described for
68 tumors *in vivo* [4,5]. Thus, these spheroids partially mimic *in vivo* tumor physiology,
69 heterogeneity, microenvironment, and drug resistance [6]. These intrinsic properties of the tumor
70 and its microenvironment restrict the extravasation, penetration, targeting and retention of drugs
71 into the tumor tissue, thus resulting in low therapeutic efficacy and severe off-target effects. To
72 overcome these limitations, the design and evaluation of efficient and targeted drug delivery
73 modalities are required to increase the local dose of anticancer drugs at the desired site while
74 reducing side effects to healthy tissues.

75 Among these modalities, microbubble-assisted ultrasound (MB-assisted US) is a promising
76 physical method for the noninvasive and targeted delivery of various types of anticancer drugs,
77 including chemotherapeutic drugs, nucleic acids (*e.g.*, plasmid DNA, mRNA, siRNA),
78 immunotherapeutics, kinase inhibitors, tumor sensitizers and oncolytic viruses [7–10]. These

79 therapeutics and MBs (*i.e.*, bare or targeted ones) can be administered intratumorally and
80 intravenously depending on the pharmacological properties of both agents and/or the desired
81 therapeutic effect [11]. The therapeutics are either coadministered or administered successively
82 with MBs *in vivo* and can also be charged on or into the MBs and be administered together. Then,
83 US is applied to the tumor tissue when a quantity of MBs and drugs are sufficiently accumulated
84 [12]. In response to US waves, MBs oscillate close to biological barriers, such as the plasma
85 membrane of tumor cells (after their intratumoral administration) or the blood-tumor barrier (after
86 their intravenous administration), therefore promoting acoustic phenomena (*e.g.*, pulling/pushing
87 processes, microstreaming, shock waves, microjet) [13]. These phenomena transiently
88 permeabilize these barriers to the therapeutics through the stimulation of intracellular (*e.g.*,
89 formation of membrane pores and endocytosis), paracellular (*e.g.*, disruption of tight junctions)
90 and transcellular (*e.g.*, transcytosis) pathways. Thus, this US modality enhances the therapeutic
91 efficacy of anticancer drugs by improving their intratumoral bioavailability while minimizing their
92 off-target effects [14].

93 Since the advent of spheroids, fewer than ten published *in vitro* studies have used spheroids
94 to either design and evaluate US protocols and new formulations of drugs and MBs or to
95 investigate the influence of the tumor microenvironment on therapeutic efficacy [1,15,16]. In this
96 context, the aims of the present study are (i) to evaluate the influence of acoustic pressure and MB
97 concentration on the delivery of a drug model into colorectal cancer (CRC) spheroids and (ii) to
98 investigate whether MB-assisted US is able to deliver different types of chemotherapeutic drugs
99 in these CRC spheroids.

100 EXPERIMENTAL SECTION

101 *Cell culture*

102 The IVISbrite[®] HCT-116 Red F-luc tumor cell line (Perkin-Elmer[®], Codolet, France) is a
103 bioluminescence-producing cell line derived from HCT-116 human colorectal carcinoma. These
104 cells were stably transduced with the redshifted firefly luciferase gene from *Luciola Italica*. They
105 were cultured in McCoy's 5A (Thermo Fisher Scientific, Waltham, MA) supplemented with 10%
106 fetal calf serum (FCS; Eurobio, Courtaboeuf, France) and 1% penicillin/streptomycin (Thermo
107 Fisher Scientific), and they were incubated at 37 °C in a humidified atmosphere with 5% CO₂.
108 This cell line has been chosen because it is the most common cell line used to generate CRC
109 spheroids uniformly and reproducibly. In addition, the physiological properties of these spheroids
110 are well documented [17,18]

111 *Spheroid formation*

112 Adapted from Griseti et al., [19] the cells were seeded at a density of 500 cells/well in a
113 96-well clear round bottom ultralow attachment (ULA) microplate (Dutscher, Bernolsheim,
114 France) and centrifuged at 500 × g for 3 min. Then, the microplate was incubated at 37 °C in a
115 humidified atmosphere in a 5% CO₂ incubator. The plastic surface of these wells is treated to
116 prevent the attachment of cells to this surface and to promote their aggregation. This ULA surface
117 enables uniform and reproducible 3D multicellular spheroid formation after 3 days. In a
118 preliminary study, a groupwise analysis of spheroid area using a Kruskal-Wallis test showed no
119 significant difference in spheroid uniformity in microplates under our experimental conditions (p
120 > 0.05; n > 400 spheroids from 6 independent experiments). In addition, the intragroup coefficients
121 of variation of spheroid area for each experiment are small (4.6 to 4.8) indicating a greater
122 reproducibility of spheroids in our experimental conditions. The spheroids were spherical and
123 cohesive and have with an average diameter of 300 ± 10 μm.

124 *Anticancer drugs and microbubbles*

125 Bleomycin sulfate (B1141000; Sigma–Aldrich, St Louis, MO) and doxorubicin
126 (D2975000; Sigma Aldrich, St Louis, MO) were dissolved in Dulbecco’s phosphate-buffered
127 saline solution (DPBS; Thermo Fisher Scientific) at a 1 mM stock solution. Irinotecan (Accord
128 Health care AG, Bottmingen, Switzerland) was a generous gift from Dr. Virginie André (Regional
129 Center of Cancerology, Henry Kaplan, CHRU de Tours, France), and its concentration was 20
130 mg/mL. Vevo MicroMarker[®] contrast agents were purchased from VisualSonics-Fujifilm Inc.
131 (Toronto, Canada) [20,21]. These agents are MBs consisting of a gaseous core of nitrogen and a
132 perfluorobutane mixture encapsulated in by a PEGylated phospholipid shell [22]. As previously
133 reported in our *in-vitro* and *in-vivo* studies, these MBs are the most effective in delivering
134 therapeutic molecules including anticancer drugs and plasmid DNA[21–23]. They were prepared
135 according to the manufacturer’s instructions at a final concentration of 2.10^9 MB/mL.

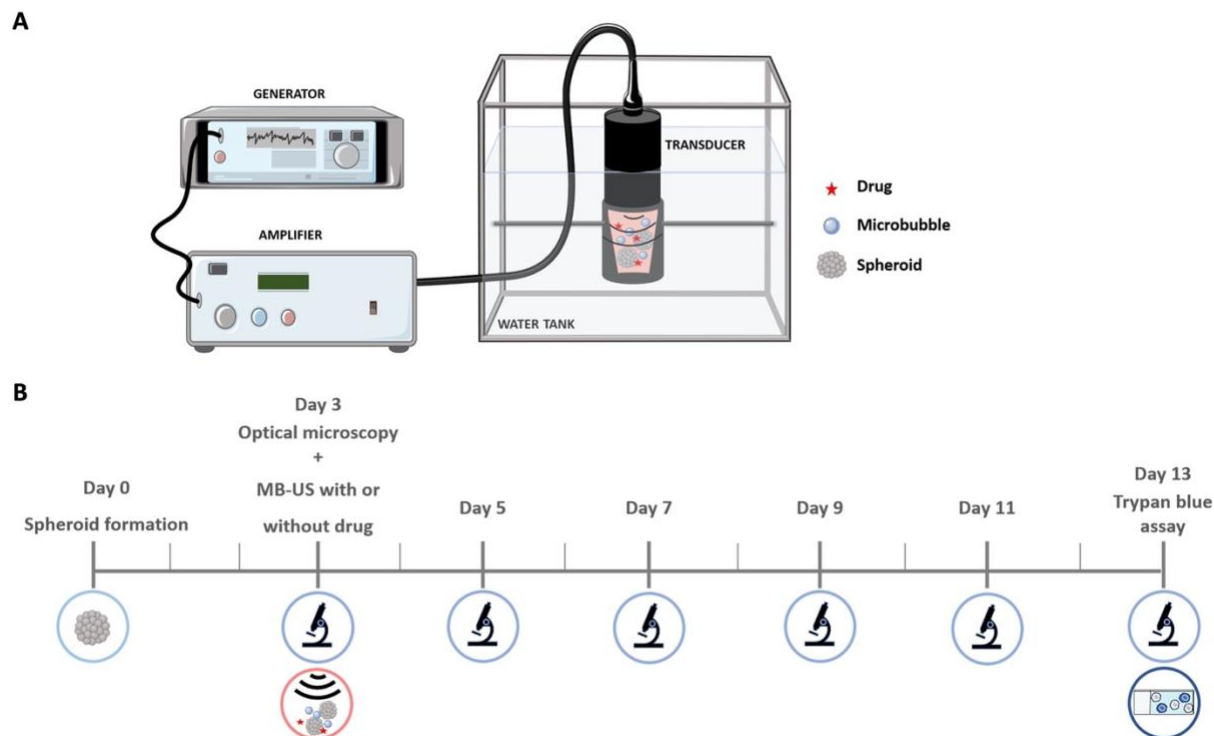
136 *Ultrasound device*

137 A 1-MHz single-element transducer (IBMF014; NDT Systems, Nashua, NH, USA) was
138 used for membrane permeabilization and drug delivery. The transducer had a diameter of 12.7
139 mm, a natural focal distance at 27 mm and a focal spot of 6 mm. An arbitrary waveform generator
140 (Agilent, Santa Clara, CA) was used to generate an electrical sinusoidal signal with a central
141 frequency of 1 MHz, pulse repetition frequency (PRF) of 10 kHz and a duty cycle of 40%. The
142 signal was then amplified using a power amplifier (AAP-500-0.2-6-D; ADECE, Veigné, France)
143 before its transmission to the transducer. A separate system using a calibrated capsule hydrophone
144 (HGL-0085; ONDA Corporation, Sunnyvale, CA, USA) was used to determine the lateral and
145 axial acoustic profiles and the sensitivity curve of the transducer. The peak negative pressures
146 (PNP) measured in the cuvette on the axis of transducer were 126, 252, 378 and 504 kPa while
147 these PNP were 100, 200, 300 and 400 kPa in water, respectively.

148 *Spheroid permeabilization*

149 Propidium iodide (PI, P4864; Sigma–Aldrich) was used as a drug model (669.39 Da;
150 hydrodynamic radius of 0.6 nm) to investigate the influence of peak negative pressure (PNP; 100,
151 200, 300 and 400 kPa) and MB concentration ($2 \cdot 10^7$, $4 \cdot 10^7$ and $8 \cdot 10^7$ MB/mL) on spheroid
152 permeabilization. This molecule is a non-permeant and fluorescent DNA intercalating agent,
153 which is commonly used as a membrane integrity marker to investigate the membrane
154 permeabilization [24–27]. This fluorescent dye has a very low fluorescent intensity in an aqueous
155 solution, while its quantum yield is 1000-fold enhanced after its intracellular uptake and its binding
156 to DNA. A suspension of 5 spheroids in 1.5 mL of McCoy’s 5A medium supplemented with 1 %
157 FCS was placed in a dedicated plastic cuvette. Then, a solution of PI (100 μ M final concentration)
158 and MBs was added to the spheroid suspension just before US exposure. The center of the cuvette
159 was immersed in a deionized and degassed water tank at 37°C, and its center was positioned at the
160 focal distance of the transducer (**Figure 1**). Subsequently, the spheroids were exposed to 1 MHz
161 sinusoid US waves with a pulse repetition period (PRP) of 100 μ s, 40 cycles per pulse (*i.e.*, 40 %
162 duty cycle) and for 1 min. Ten minutes later, the penetration and intracellular accumulation of PI
163 into spheroids were assessed using a fluorescence microscope (EVOS, M5000, Thermo Fisher
164 Scientific). A semi-quantitative analysis of microscopic images was performed with ImageJ
165 software (NIH, Bethesda, MA) in order to determine the integrated intensity of PI (a.u./ μ m²).
166 Representative confocal images of permeabilized spheroids were obtained using LEICA SP8
167 gSTED confocal microscope (Leica, Wetzlar, Germany).

168 The spheroids were exposed to MB-assisted US in the absence of PI in order to assess the
169 effects of acoustically mediated membrane permeabilization on the spheroid growth and viability
170 following the protocols described below.



171
 172 **Figure 1.** Set up and experimental timeline. (A) *In vitro* US setup. (B) Timeline of acoustically mediated drug delivery
 173 experiments on CRC spheroids.

174 *Drug Delivery*

175 Three chemotherapeutic drugs, including bleomycin (0.1 μM and 1 μM), doxorubicin (1
 176 μM and 10 μM) and irinotecan (0.1 $\mu\text{g/mL}$ and 1 $\mu\text{g/mL}$), were acoustically delivered (1 MHz,
 177 100 μs PRP, 40 cycles/pulse for 1 min in the presence of $4 \cdot 10^7$ MB/mL) into the spheroids using
 178 the same US protocol and setup described above for spheroid permeabilization. The concentrations
 179 of drugs were selected based on our *in vitro* preliminary studies. Ten minutes after US exposure,
 180 the spheroids were transferred to a 96-well ULA microplate. The final concentrations of FCS and
 181 antibiotics were increased to 10% and 1%, respectively. Finally, the microplate was incubated at
 182 37 $^{\circ}\text{C}$ in a humidified atmosphere in a 5% CO_2 incubator for spheroid growth.

183 *Spheroid growth*

184 Spheroid growth was monitored by optical microscopy (EVOS, M5000) every two days
185 for ten days after US exposure. Then, the spheroid area was measured using ImageJ software.

186 *Spheroid viability*

187 On the 13th day post-US exposure, spheroid viability was assessed using the trypan blue
188 exclusion assay. Briefly, the spheroids were harvested and washed with PBS. The spheroids were
189 pooled in two groups and incubated with 50 μ L of Accumax (Thermo Fisher Scientific) for 15 min
190 at 37 °C in a humidified atmosphere in a 5% CO₂ incubator for enzymatic dissociation. Then, they
191 were dissociated mechanically (rapid pipetting) to generate a cell suspension. One volume of cells
192 was mixed with an equal volume of trypan blue. Finally, the concentration of viable cells was
193 measured using a CountessTM automated cell counter (Invitrogen, Waltham, MA).

194 *Transmission electron microscopy*

195 As previously reported [28], the spheroids were fixed in 1% glutaraldehyde and 4%
196 paraformaldehyde (Sigma–Aldrich) in 0.1 M phosphate buffer (pH 7.2) for 24 h. Then, the samples
197 were washed in PBS and postfixed in 2% buffered osmium tetroxide (Agar Scientific, Stansted,
198 UK) for 1 h. After dehydration in a graded series of ethanol solutions (70% and 90% v/v) and
199 propylene oxide (100%), an impregnation step was performed with a mixture of propylene
200 oxide/Epon resin (1:1; Sigma–Aldrich) and then left overnight in pure resin. The samples were
201 then embedded in Epon resin (Sigma–Aldrich), which was allowed to polymerize for 48 h at 60
202 °C. Thin (250 nm) and ultrathin sections (90 nm) of these blocks were generated with a Leica EM
203 UC7 ultramicrotome (Leica, Wetzlar, Germany). Thin sections were stained with 0.5% toluidine
204 blue (Sigma–Aldrich), and ultrathin sections were stained with 2% uranyl acetate (Agar Scientific
205 Ltd, Stansted, UK) and 5% lead citrate (Sigma–Aldrich). The microscopic observations were made
206 with a transmission electron microscope (JEOL 1011, Tokyo, Japan).

207 *Statistical analysis*

208 All quantitative data were analyzed using Kruskal–Wallis’s test and Dunn's multiple
209 comparison test for spheroid permeabilization and viability and two-way ANOVA and Dunnett’s
210 test for spheroid growth (significance was defined as $p < 0.05$) with GraphPad Prism v.9.5.1
211 (GraphPad Software Inc., La Jolla, CA).

212 RESULTS

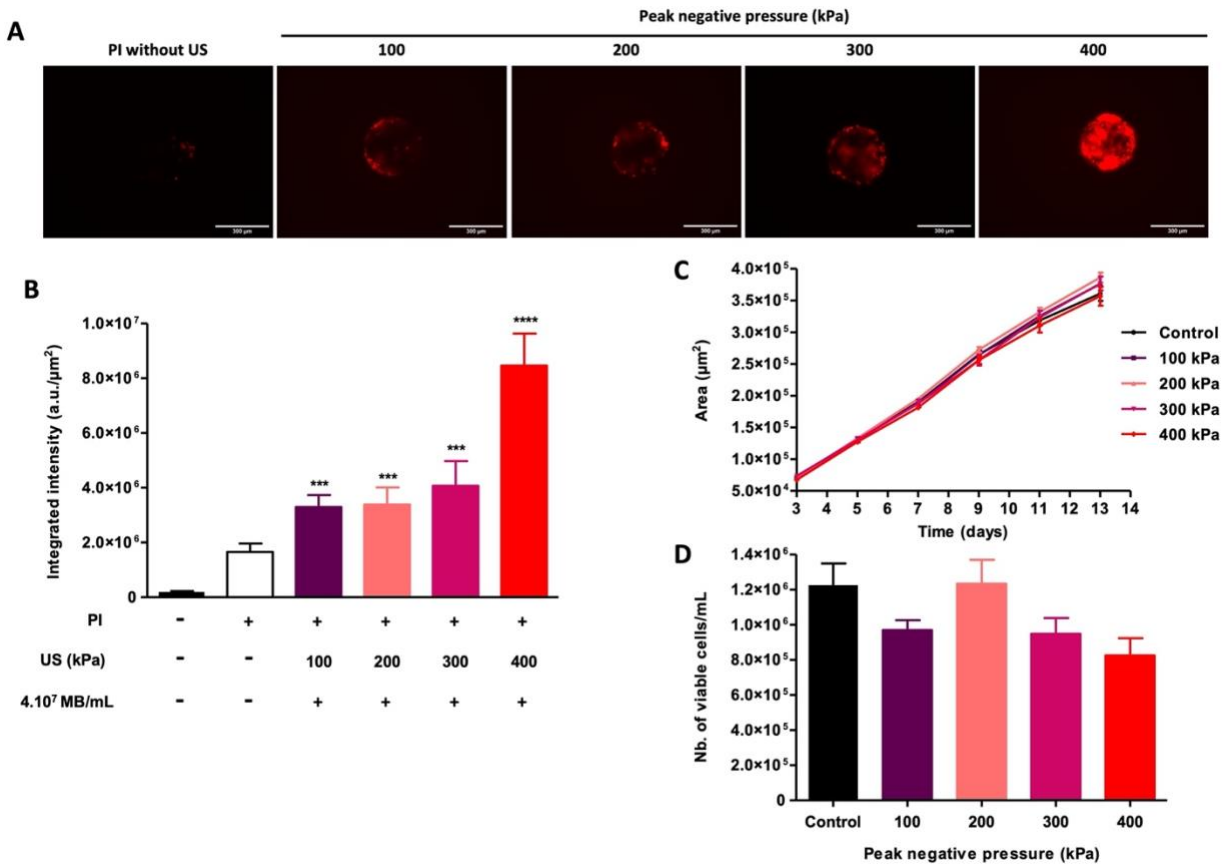
213 *CRC spheroid permeabilization to small molecules*

214 To evaluate the influence of PNP and MB concentration on the permeabilization level of
215 CRC spheroids, the membrane permeabilization of tumor cells was monitored using a small and
216 nonpermeant drug model, PI, and the permeabilization level was assessed by epifluorescence
217 microscopy.

218 As depicted in **Figures 2A** and **2B**, the simple incubation of spheroids with PI revealed the
219 presence of fluorescence labeling ($1.7 \pm 0.3 \times 10^6$ a.u./ μm^2) inside the spheroids corresponding to
220 the presence of dead cells. The exposure of spheroids to 100 kPa in the presence of MBs
221 (4×10^7 MB/mL) significantly increased their permeabilization to PI compared to PI incubation
222 alone ($***p < 0.001$; $3.3 \pm 0.4 \times 10^6$ versus $1.7 \pm 0.3 \times 10^6$ a.u./ μm^2). The increase in the acoustic
223 pressure from 200 to 300 kPa caused spheroid permeabilization similar to that at an acoustic
224 pressure of 100 kPa ($p > 0.05$; $3.4 \pm 0.6 \times 10^6$ and $4.1 \pm 0.9 \times 10^6$ a.u./ μm^2 , respectively).
225 However, the exposure of spheroids to 400 kPa induced a 2.5-fold increase in their
226 permeabilization in comparison to their exposure to 100 kPa ($****p < 0.0001$; $8.5 \pm 1.2 \times 10^6$
227 versus $3.3 \pm 0.4 \times 10^6$ a.u./ μm^2).

228 The influence of this range of PNP (from 100 to 400 kPa) on spheroid growth and viability
229 was investigated by optical microscopy over 13 days and using a trypan blue exclusion assay on

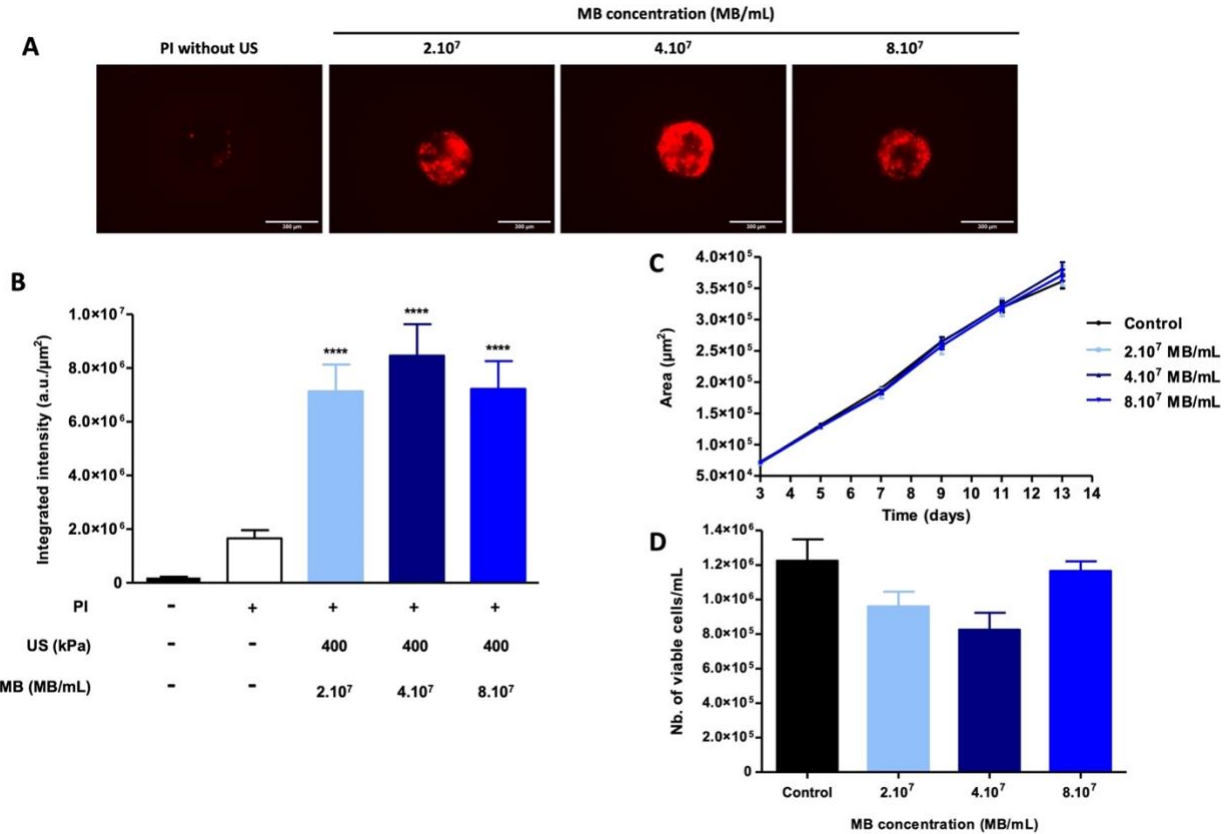
230 the 13th day of spheroid growth, respectively. The increase in PNP had no significant influence on
 231 spheroid growth (**Figure 2C**) or viability (**Figure 2D**).



232
 233 **Figure 2.** Influence of peak negative pressure (PNP) on CRC spheroid permeabilization, growth and viability. CRC
 234 spheroids were incubated with 100 μM PI alone or with MB-assisted US at 100 to 400 kPa for 1 min. (A)
 235 Representative fluorescence images of permeabilized spheroids. The scale bar indicates 300 μm . (B) Quantification
 236 of PI fluorescence intensity of permeabilized spheroids. Data expressed as mean \pm SEM was calculated from 18 CRC
 237 spheroids. Statistical analysis was performed using Kruskal–Wallis’s test and Dunn’s multiple comparison test.
 238 Significance was defined as $p < 0.05$ (** $p < 0.001$, *** $p < 0.0001$). Then, CRC spheroids were exposed to MB-
 239 assisted US at 100 to 400 kPa for 1 min. (C) The spheroid growth was assessed over time using optical imaging. Data
 240 expressed as mean \pm SEM was calculated from 18 CRC spheroids. Statistical analysis was performed using Two-way
 241 ANOVA test and Dunnett’s test. Significance was defined as $p < 0.05$ (D) The spheroid viability was evaluated on the
 242 13th day post-US exposure, using trypan blue dye exclusion assay. Data expressed as mean \pm SEM was calculated

243 from 18 CRC spheroids. Statistical analysis was performed using Kruskal–Wallis’s test and Dunn’s multiple
244 comparison test. Significance was defined as $p < 0.05$.

245 Then, the influence of MB concentration ($2 \cdot 10^7$, $4 \cdot 10^7$ and $8 \cdot 10^7$ MB/mL) on spheroid
246 permeabilization to PI was investigated at the given PNP of 400 kPa using the same experimental
247 strategy as shown in **Figures 3A** and **3B**. As described above, the coincubation of spheroids with
248 PI stained the dead cells, thus causing an increase in the associated fluorescence intensity
249 ($1.7 \pm 0.3 \times 10^6$ a.u./ μm^2). The insonation of spheroids in the presence of MBs at $2 \cdot 10^7$ MB/mL
250 led to a significant permeabilization of spheroids compared to PI incubation alone
251 ($****p < 0.0001$; $7.1 \pm 1 \times 10^6$ *versus* $1.7 \pm 0.3 \times 10^6$ a.u./ μm^2). Surprisingly, the doubling or
252 quadrupling of the MB concentration resulted in similar permeabilization of spheroids as for an
253 MB concentration of $2 \cdot 10^7$ MB/mL ($p > 0.05$; $8.5 \pm 1.1 \times 10^6$ and $7.2 \pm 1 \times 10^6$ a.u./ μm^2 ,
254 respectively). In addition, the increase in MB concentration from $2 \cdot 10^7$ to $8 \cdot 10^7$ MB/mL did not
255 affect either spheroid growth over time (**Figure 3C**) or viability on the 13th day (**Figure 3D**).
256 Altogether, these data show that MB-assisted US permeabilizes CRC spheroids without affecting
257 their growth and viability under our experimental conditions.



258

259 **Figure 3.** Influence of MB concentration on CRC spheroid permeabilization, growth and viability. CRC spheroids

260 were incubated with 100 μM PI alone or with MB-assisted US at 400 kPa for 1 min in the presence of 2.10⁷, 4.10⁷ or

261 8.10⁷ MB/mL. (A) Representative fluorescence images of permeabilized spheroids. The scale bar indicates 300 μm.

262 (B) Quantification of PI fluorescence intensity of permeabilized spheroids. Data expressed as mean ± SEM was

263 calculated from 18 CRC spheroids. Statistical analysis was performed using Kruskal–Wallis’s test and Dunn’s

264 multiple comparison test. Significance was defined as $p < 0.05$ (**** $p < 0.0001$). CRC spheroids were incubated with

265 100 μM PI alone or with MB-assisted US at 400 kPa for 1 min in the presence of 2.10⁷, 4.10⁷ or 8.10⁷ MB/mL. (C)

266 The spheroid growth was assessed over time using optical imaging. Data expressed as mean ± SEM was calculated

267 from 18 CRC spheroids. Statistical analysis was performed using Two-way ANOVA test and Dunnett’s test.

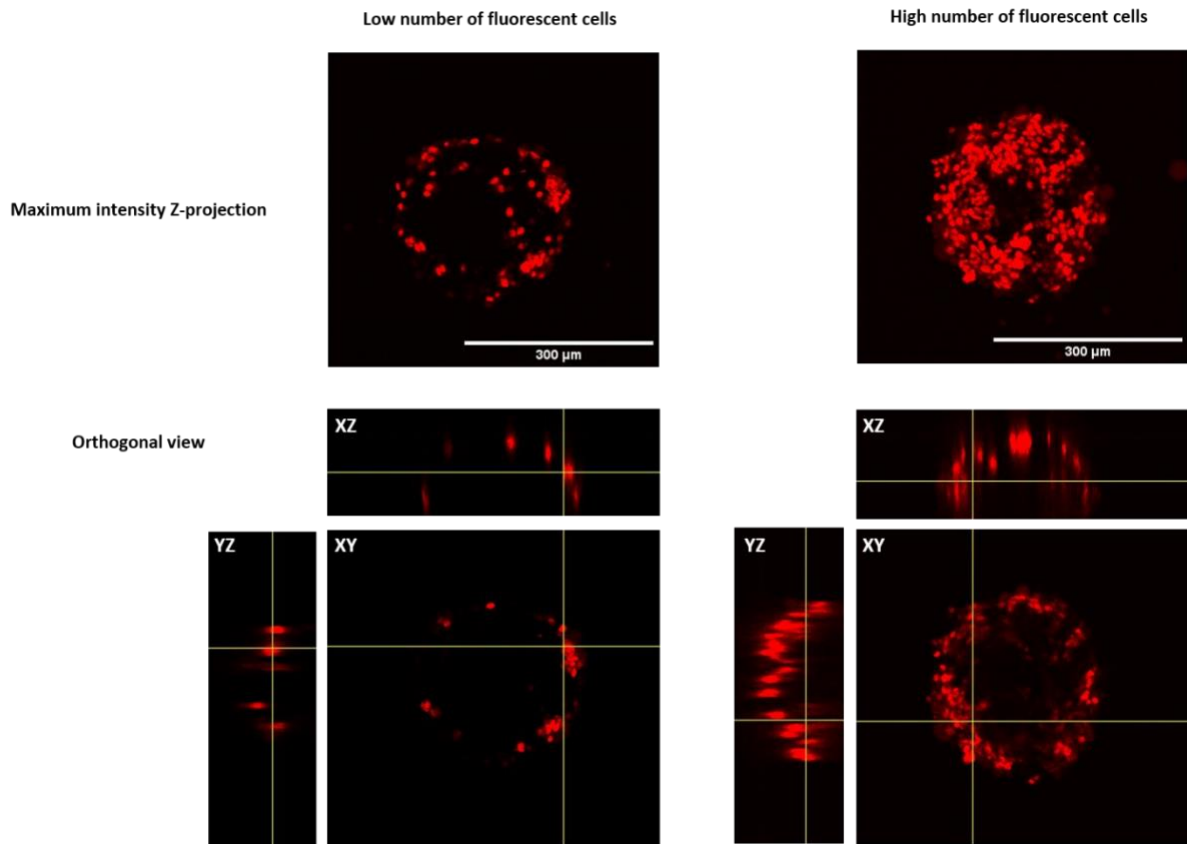
268 Significance was defined as $p < 0.05$ (D) The spheroid viability was evaluated on the 13th day post-MB-assisted US

269 exposure, using trypan blue dye exclusion assay. Data expressed as mean ± SEM was calculated from 18 CRC

270 spheroids. Statistical analysis was performed using Kruskal–Wallis’s test and Dunn’s multiple comparison test.

271 Significance was defined as $p < 0.05$.

272 In addition, our confocal microscopic observations of permeabilized spheroids revealed
273 heterogeneous permeabilization between the spheroids and within each spheroid. Indeed, the
274 spheroids showed a low or high number of fluorescent cells predominantly located in the outer cell
275 layer of spheroids (**Figure 4**).

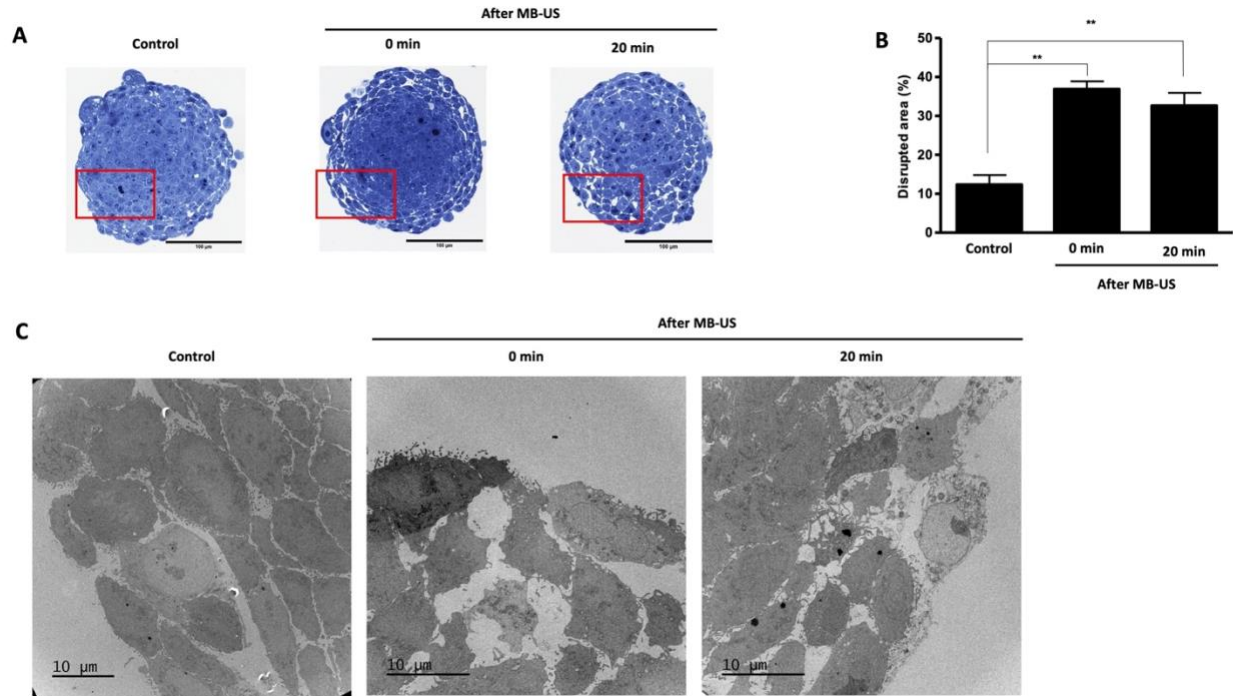


276
277 **Figure 4. Representative confocal images of permeabilized spheroids.** The scale bar indicates 300 μm.

278 *Impact of US-MB on spheroid structure*

279 Using the same setup and experimental conditions (400 kPa PNP, $4 \cdot 10^7$ MB/mL)
280 previously described for spheroid permeabilization, ultrastructural modifications of CRC
281 spheroids were investigated using both histology after toluidine blue staining (**Figures 5A and**
282 **5B**) and transmission electron microscopy (TEM; **Figure 5C**) immediately and 20 min after MB-
283 assisted US (in the absence of PI). Optical images of control spheroids (no MB-assisted US

284 exposure) revealed no visually apparent effects on spheroid morphology (**Figure 5A**). In the
285 control condition, few intercellular disruptions were observed in the peripheral layers of tumor
286 cells, which could be attributed to the putative artifactual effect of sample preparation and handling
287 (**Figures 5A and 5B**). However, the spheroids appeared less cohesive in structure immediately
288 after MB-assisted US exposure compared to the control spheroids (**Figure 5A**). The intercellular
289 junctions of tumor cells located in the peripheral layers of spheroids were significantly disrupted
290 in comparison to the control spheroids (** $p < 0.01$; $37 \pm 2\%$ versus $12 \pm 2\%$; **Figure 5B**). A
291 slight but nonsignificant decrease in this acoustically disrupted area was observed 20 min after
292 US-assisted MB exposure ($p > 0.05$; $32 \pm 3\%$ versus $37 \pm 2\%$; **Figure 5B**). One noticed that MB-
293 assisted US did not seem to affect the structure of the intermediate layer or the core of spheroids
294 under our experimental conditions. Moreover, TEM analysis confirmed these histological
295 observations. The sonicated spheroids exhibited significant changes in cell morphology and
296 organization (*i.e.*, wide intercellular gaps) in the peripheral layer of spheroids, which resulted in
297 loss of spheroid cohesion in this layer compared to the control (**Figure 5C**). These results
298 demonstrate that MB-assisted US affects only the peripheral layer of CRC spheroids.



299

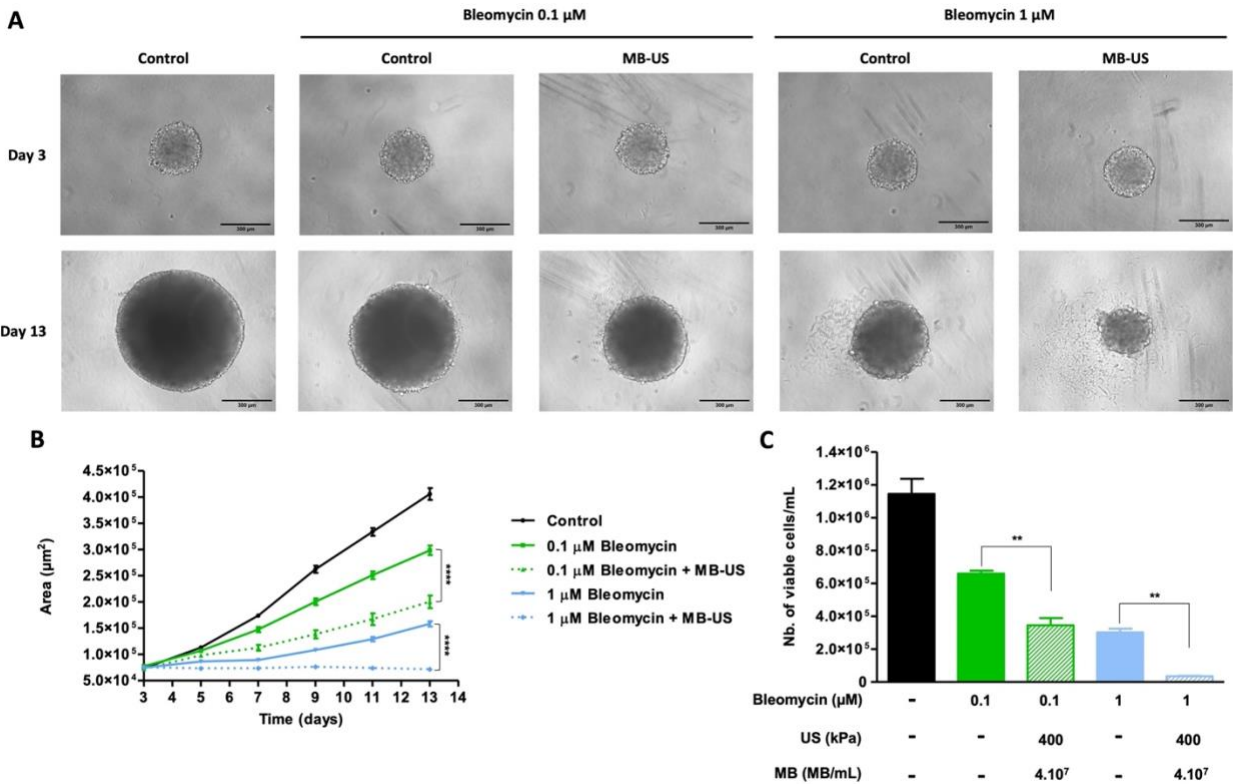
300 **Figure 5.** Effects of MB-assisted US on spheroid structure. (A) Representative optical images of CRC spheroid slices
 301 stained with toluidine blue, immediately or 20 min after MB-assisted US exposure (MB concentration: 4.10^7 MB/mL,
 302 US parameters: 400 kPa for 1 min). The scale bar indicates 100 μ m. The red square shows peripheral layer of CRC
 303 spheroids. (B) Percentage of the disrupted spheroid area after MB-assisted US exposure. Data expressed as mean \pm
 304 SEM was calculated from 12 CRC spheroids. Statistical analysis was performed using Kruskal–Wallis’s test and
 305 Dunn’s multiple comparison test. Significance was defined as $p < 0.05$ (** $p < 0.01$). (C) Representative TEM images
 306 of disrupted area of CRC spheroids. The scale bar indicates 10 μ m.

307 *Drug delivery using MB-assisted US*

308 Three anticancer drugs, bleomycin, doxorubicin and irinotecan, were acoustically delivered
 309 at two different concentrations inside CRC spheroids using the US setup and parameters (400 kPa
 310 PNP, 4.10^7 MB/mL). The cytotoxic effects of such drugs were investigated by monitoring spheroid
 311 growth over 13 days under optical microscopy and by assessing spheroid viability on the 13th day
 312 using a trypan blue exclusion assay.

313 **Figure 6A** displays microscopy images of control spheroids (*i.e.*, no treatment) and
314 spheroids treated once either with bleomycin alone or with bleomycin delivered using MB-assisted
315 US (*i.e.*, 0.1 and 1 μM bleomycin). As shown in this figure, the spheroid size and morphology
316 were highly uniform between all treatment groups on the 3rd day (*i.e.*, images acquired before the
317 treatment). This good reproducibility of our spheroid model enabled us to clearly assess their
318 cytotoxic effects over time; here, only the last day of follow-up is shown. Control spheroids
319 exhibited linear growth, and the spheroid-doubling time was close to 5 days (**Figure 6B**). The
320 incubation of spheroids with 0.1 μM bleomycin significantly reduced spheroid growth over 13
321 days without inducing spheroid destruction compared to the control condition ($****p < 0.0001$).
322 Consequently, the spheroid-doubling time increased to 6 days. The acoustically mediated delivery
323 of bleomycin at 0.1 μM led to an additional and significant reduction in spheroid growth (without
324 inducing spheroid destruction) in comparison with bleomycin treatment alone ($****p < 0.0001$).
325 This reduction in spheroid growth was associated with the prolongation of spheroid-doubling time,
326 *i.e.*, 7 days. The increase in bleomycin concentration from 0.1 to 1 μM significantly accentuated
327 the slowdown of spheroid growth ($****p < 0.0001$; **Figure 6B**) without causing spheroid
328 destruction and increased the spheroid-doubling time to 9 days. One noticed that the therapeutic
329 efficacy of acoustically mediated delivery of bleomycin at 0.1 μM is close to that obtained with
330 bleomycin treatment alone at 1 μM ($p > 0.05$). The exposure of spheroids to MB-assisted US in
331 the presence of 1 μM bleomycin completely inhibited their growth compared to the bleomycin
332 treatment alone ($****p < 0.0001$). On the 13th day, the trypan blue exclusion assay confirmed these
333 results (**Figure 6C**). The acoustically mediated delivery of 0.1 μM bleomycin induced a 2-fold
334 decrease in spheroid viability compared to bleomycin treatment alone ($**p < 0.01$). This reduction
335 in spheroid viability was similar to that caused by the treatment of spheroids with 1 μM bleomycin

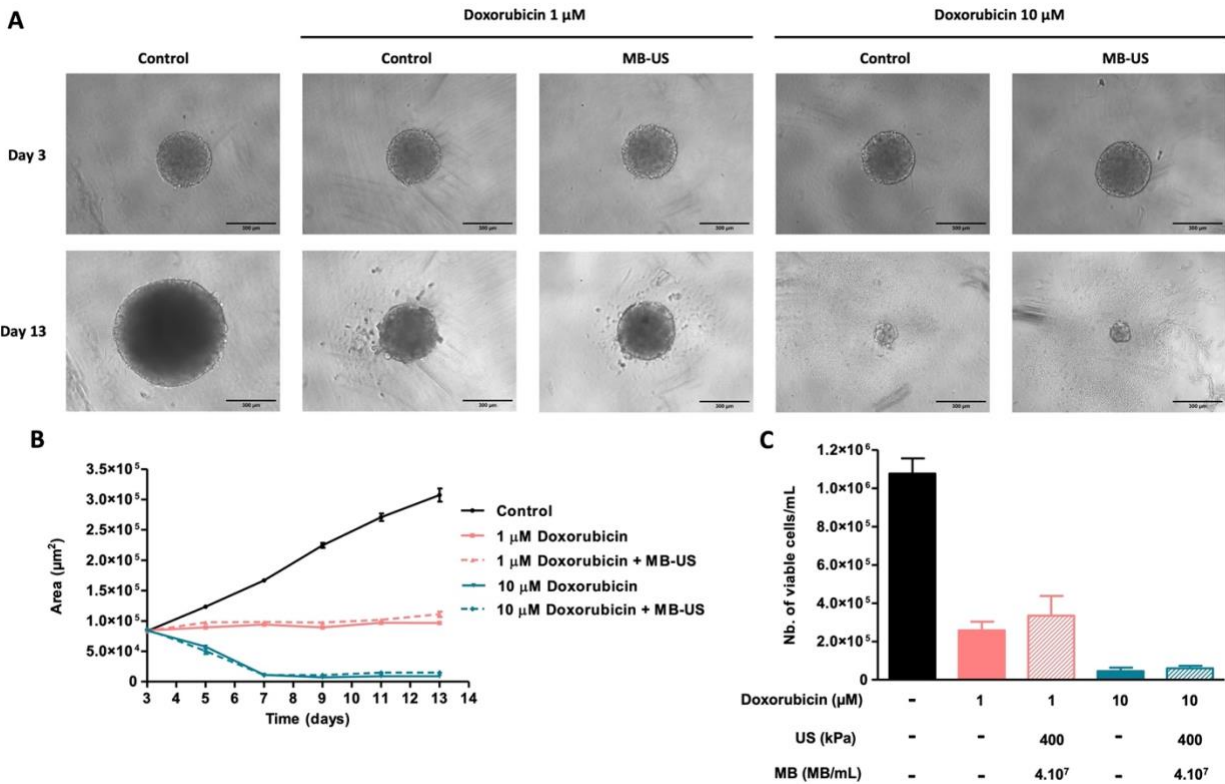
336 alone ($p > 0.05$). As expected, the delivery of 1 μM bleomycin using MB-assisted US significantly
 337 decreased spheroid viability compared to bleomycin treatment alone at 1 μM (** $p < 0.01$). These
 338 results show that MB-assisted US potentiates the cytotoxic effect of bleomycin on CRC spheroids.



339
 340 **Figure 6.** Bleomycin delivery using MB-assisted US. CRC spheroids were incubated with 0.1 or 1 μM bleomycin
 341 alone or with MB-assisted US at 400 kPa for 1 min in the presence of 4.10^7 MB/mL. (A) Representative optical images
 342 of CRC spheroids before (Day 3) and 10 days after treatment (Day 13). The scale bar indicates 300 μm . (B) The
 343 spheroid growth was assessed over time using optical imaging. Data expressed as mean \pm SEM was calculated from
 344 8 CRC spheroids. Statistical analysis was performed using Two-way ANOVA test and Dunnett's test. Significance
 345 was defined as $p < 0.05$ (**** $p < 0.0001$). (C) The spheroid viability was evaluated on the 13th day post- MB-assisted
 346 US exposure, using trypan blue dye exclusion assay. Statistical analysis was performed using Kruskal–Wallis's test
 347 and Dunn's multiple comparison test. Significance was defined as $p < 0.05$ (** $p < 0.01$).

348 As shown in **Figure 7**, the cytotoxic effect of the acoustically mediated delivery of
 349 doxorubicin (*i.e.*, 1 and 10 μM) was investigated following the same protocol reported above. As

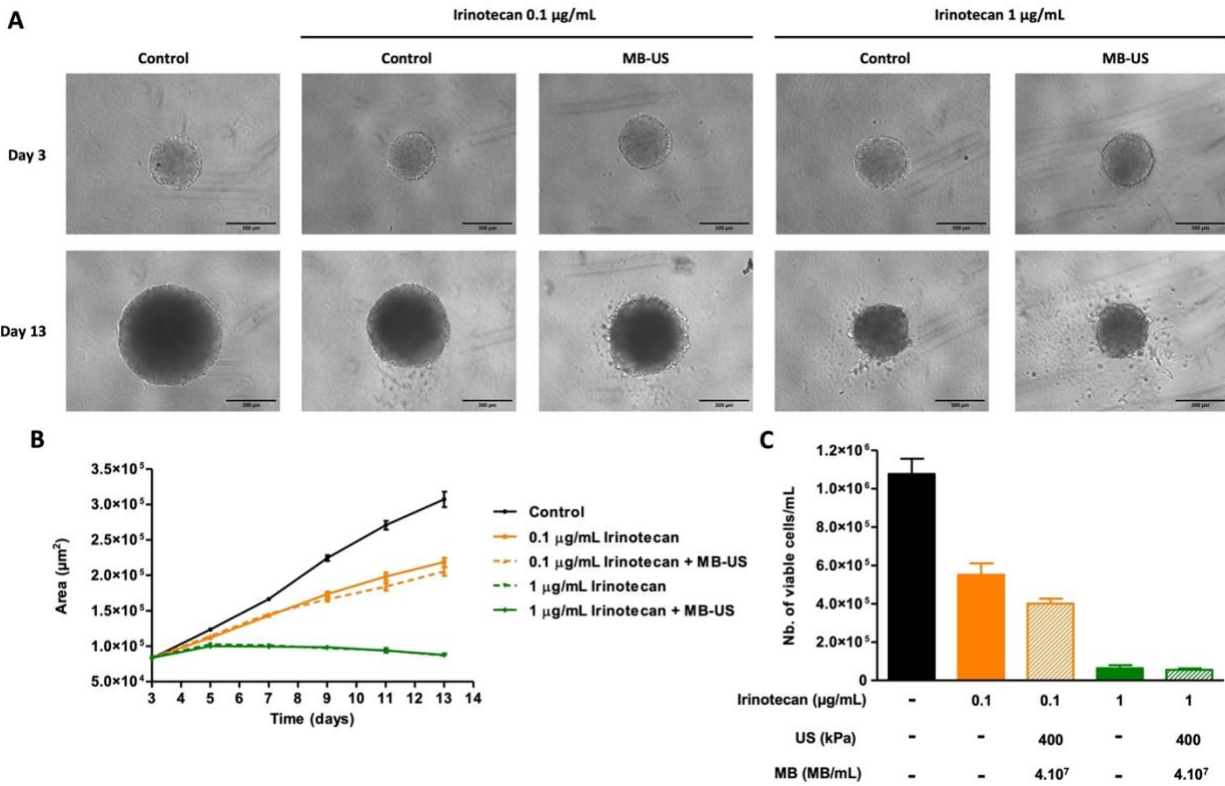
350 previously described, control spheroids displayed linear growth with a doubling time close to 5
351 days (**Figures 7A and 7B**). Doxorubicin treatment alone at 1 μM induced complete inhibition of
352 spheroid growth ($****p < 0.0001$; **Figures 7A and 7B**), while treatment with a 10-fold higher
353 concentration induced a significant reduction in spheroid area related to an almost complete
354 destruction of the spheroid compared to control spheroids ($****p < 0.0001$; **Figures 7A and 7B**).
355 Regardless of the doxorubicin concentration, its cytotoxic effect was not potentiated when this
356 anticancer drug was delivered using MB-assisted US inside the spheroids ($p > 0.05$). These data
357 were also confirmed by trypan blue exclusion assay on Day 13 (**Figure 7C**). Doxorubicin
358 treatment alone at 1 μM led to a 3.8-fold decrease in spheroid viability compared to the control
359 condition ($***p < 0.001$; $2.6 \pm 0.4 \times 10^5$ versus $1.0 \pm 0.08 \times 10^6$ viable cells/mL). The acoustically
360 mediated delivery of 1 μM doxorubicin did not result in an additional reduction in spheroid
361 viability in comparison to doxorubicin treatment alone ($p > 0.05$). Similarly, 10 μM doxorubicin
362 delivered or not using MB-assisted US induced a comparable decrease in spheroid viability
363 ($p > 0.05$; $6.0 \pm 1.2 \times 10^4$ versus $4.5 \pm 1.8 \times 10^4$ viable cells/mL). Altogether, these data reveal that
364 under our experimental conditions, MB-assisted US does not increase the cytotoxic effect of
365 doxorubicin on CRC spheroids at either selected concentration.



366
 367 **Figure 7.** Doxorubicin delivery using MB-assisted US. CRC spheroids were incubated with 1 or 10 μM doxorubicin
 368 alone or with MB-assisted US at 400 kPa for 1 min in the presence of 4.10^7 MB/mL. (A) Representative optical images
 369 of CRC spheroids before (Day 3) and 10 days after treatment (Day 13). The scale bar indicates 300 μm . (B) The
 370 spheroid growth was assessed over time using optical imaging. Data expressed as mean \pm SEM was calculated from
 371 8 CRC spheroids. Statistical analysis was performed using Two-way ANOVA test and Dunnett's test. Significance
 372 was defined as $p < 0.05$. (C) The spheroid viability was evaluated on the 13th day post- MB-assisted US exposure,
 373 using trypan blue dye exclusion assay. Statistical analysis was performed using Kruskal–Wallis's test and Dunn's
 374 multiple comparison test. Significance was defined as $p < 0.05$.

375 Moreover, the CRC spheroids were treated with irinotecan at 0.1 $\mu\text{g/mL}$ or 1 $\mu\text{g/mL}$ alone
 376 or delivered using MB-assisted US. Once again, the spheroids exhibited linear growth with a
 377 doubling time close to 5 days under control conditions (**Figures 8A** and **8B**). At a 0.1 $\mu\text{g/mL}$
 378 concentration, slower spheroid growth was observed compared to the control condition
 379 ($****p < 0.0001$; **Figures 8A** and **8B**). The acoustically mediated delivery of such irinotecan

380 concentration induced a slightly more important reduction of spheroid growth compared to the
381 0.1 µg/mL irinotecan treatment alone, but this result was not significant ($p > 0.05$). The incubation
382 of spheroids with 1 µg/mL irinotecan alone resulted in a complete inhibition of spheroid growth
383 without generating their destruction in comparison to the control condition (**** $p < 0.0001$;
384 **Figures 8A** and **8B**). Unfortunately, the delivery of such irinotecan concentrations using MB-
385 assisted US did not lead to an additional and significant decrease in spheroid growth compared to
386 irinotecan treatment alone ($p > 0.05$). The trypan blue exclusion assay supported these results
387 (**Figure 8C**). The acoustically mediated delivery of 0.1 µg/mL irinotecan caused a slight but
388 nonsignificant decrease in spheroid viability in comparison to 0.1 µg/mL irinotecan treatment
389 alone ($p > 0.05$; $4.0 \pm 0.3 \times 10^5$ versus $5.5 \pm 0.6 \times 10^5$ viable cells/mL). No significant decrease in
390 spheroid viability was observed between their treatment with 1 µg/mL irinotecan alone or
391 delivered using MB-assisted US ($p > 0.05$; $6.0 \pm 1.5 \times 10^4$ versus $5.5 \pm 0.7 \times 10^4$ viable cells/mL).
392 These results demonstrate that under our experimental conditions, MB-assisted US does not
393 potentiate the cytotoxic effect of irinotecan on CRC spheroids regardless of its selected
394 concentration.



395
 396 **Figure 8.** Irinotecan delivery using MB-assisted US. CRC spheroids were incubated with 0.1 or 1 µg/mL irinotecan
 397 alone or with MB-assisted US at 400 kPa for 1 min in the presence of 4.10⁷ MB/mL. (A) Representative optical images
 398 of CRC spheroids before (Day 3) and 10 days after treatment (Day 13). The scale bar indicates 300 µm. (B) The
 399 spheroid growth was assessed over time using optical imaging. Data expressed as mean ± SEM was calculated from
 400 8 CRC spheroids. Statistical analysis was performed using Two-way ANOVA test and Dunnett’s test. Significance
 401 was defined as p < 0.05. (C) The spheroid viability was evaluated on the 13th day post-MB-assisted US exposure,
 402 using trypan blue dye exclusion assay. Statistical analysis was performed using Kruskal–Wallis’s test and Dunn’s
 403 multiple comparison test. Significance was defined as p < 0.05.

404 **DISCUSSION**

405 The aim of the present study was to evaluate the efficacy of MB-assisted US for the delivery
 406 of anticancer drugs to CRC spheroids. First, the influence of PNP and MB concentration on the
 407 permeabilization of these spheroids to small molecules was assessed using PI as a drug model. Our
 408 results show that MB-assisted US significantly increases the delivery of this drug model into CRC

409 spheroids (**Figures 2A and 2B**). As previously reported for cell suspensions or *in vivo*, the
410 permeabilization efficiency depends on PNP [29–31]. The increase in PNP induces a gradual
411 permeabilization of spheroids, and a maximum permeabilization efficiency is reached at a PNP of
412 400 kPa. In future experiments, it could be relevant to investigate in depth the influence of other
413 US parameters on the permeabilization of spheroids. Surprisingly, the increase in MB
414 concentration did not affect the permeabilization efficiency of spheroids (**Figures 3A and 3B**).
415 The data available in the literature showed that the permeabilization of cells and tissues is
416 dependent on the MB concentration [32–34]. In the near future, the influence of a wider range of
417 MB concentrations as well as the type of MBs (*i.e.*, soft- vs. hard-shelled MBs, bare vs. targeted
418 MBs, poly- vs. mono-disperse MBs, *etc.*) on spheroid permeabilization will be evaluated with our
419 US setup. The 3D view of permeabilized spheroids using confocal fluorescence microscopy
420 allowed accurate location of permeabilized cells in the peripheral layer of spheroids (**Figure 4**).
421 Such spheroid phenotype with more or less significant number of permeabilized cells is the most
422 frequently observed phenotype in previous studies. Nevertheless, Paškevičiūtė et al.[35] reported
423 that MB-assisted US enhanced the permeabilization of peripheral and middle layers to doxorubicin
424 (anticancer fluorescent drug, 544 Da) in lung and breast cancer spheroids. This difference observed
425 between our study and those published may be related to the US setup and parameters, MBs (*e.g.*,
426 type, dose, *etc.*), tumor cell line and the dye used as the model drug.

427 Subsequently, we investigated the bioeffects of MB-mediated US on the architecture of
428 spheroids using TEM and histology after toluidine blue staining. MB-assisted US strongly altered
429 the peripheral cell layers of spheroids. The shape of the tumor cells was modified, and the
430 intercellular junctions were disrupted from the spheroid surface to a depth of 70 nm immediately
431 after US exposure as well as 20 min later (**Figure 5**). These results suggest that the mechanical

432 actions of cavitating MBs take place on the surface and in the outer layers of the spheroids. Due
433 to their micrometric size, the MBs would not diffuse inside the spheroids. To confirm this
434 hypothesis, spheroid permeabilization in the presence of fluorescent MBs and PI could be
435 conducted in real time under a confocal microscope. In addition, our TEM results confirmed our
436 confocal microscopic observations of permeabilized spheroids. This preliminary electron
437 microscopy study is, to our knowledge, the first of its kind in the field of acoustically mediated
438 drug delivery into spheroids.

439 Moreover, we assessed the ability of MB-assisted US to deliver chemotherapeutic drugs,
440 including bleomycin, doxorubicin and irinotecan, into CRC spheroids. These spheroids were
441 treated with two different drug concentrations and then exposed or not to MB-assisted US. The
442 results showed that the cytotoxic effect of bleomycin was potentiated when this drug was delivered
443 using MB-assisted US (**Figure 6**). In agreement with published data, these results indirectly
444 demonstrated that the increased cytotoxicity of bleomycin could be ascribed to an enhancement in
445 its intracellular uptake through acoustically induced hydrophilic pores [36,37]. The transport of
446 bleomycin across the plasma membrane of tumor cells is governed by the receptor-mediated
447 endocytosis process [38]. The low number of these membrane receptors exposed at the cell surface
448 limits the intracellular accumulation of bleomycin and therefore its cytotoxicity. The exposure of
449 spheroids to MB-assisted US leads to an increased membrane permeability of tumor cells and
450 enables the direct access of bleomycin to their cytoplasm, where its molecular targets are located.
451 These results are in agreement with previous studies conducted *in vitro* on different human and
452 murine tumor cell lines (*i.e.*, gingival squamous carcinoma, melanoma, glioblastoma and
453 colorectal cancer) [39–41] and *in vivo* (*i.e.*, gingival squamous carcinoma and melanoma) [39,40].
454 The acoustically mediated delivery of bleomycin induces a 50% to 80% decrease in cell viability

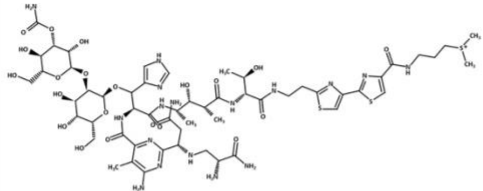
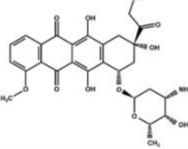
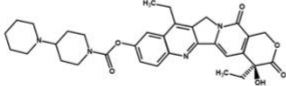
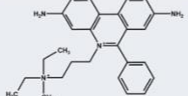
455 regardless of the cell line used and experimental conditions (*i.e.*, cell suspension *versus* adherent
456 cells, type and dose of MBs, bleomycin concentration and US parameters). *In vivo*, Iwanaga et al.
457 reported that the repeated delivery of a low bleomycin dose (10 µg) using MB-assisted US led to
458 a near disappearance of the tumor in a murine squamous carcinoma model without inducing severe
459 side effects [39]. Altogether, these results suggest that spheroids could be a suitable predictive and
460 complementary tumor model between *in vitro* and *in vivo* models.

461 Surprisingly, MB-assisted US did not potentiate the cytotoxic effects of doxorubicin and
462 irinotecan on CRC spheroids under our experimental conditions (**Figures 7 and 8**). The first
463 hypothesis, which could explain these results, relies on the intrinsic properties of these anticancer
464 drugs (**Table 1**). Doxorubicin and irinotecan are low molecular weight molecules (< 600 Da) that
465 can passively cross the plasma membrane of tumor cells, while bleomycin (> 1 400 Da) requires
466 a receptor-mediated endocytosis process. In addition, the lipophilicity of these anticancer
467 molecules is also a physico-chemical parameter, which must be considered because it plays a major
468 role in their pharmacological properties (pharmacokinetics, pharmacodynamics, tissue
469 biodistribution, *etc.*) [42]. Doxorubicin and irinotecan are more lipophilic than bleomycin [43,44].
470 As a result, MB-assisted US would not significantly enhance the intracellular concentrations of
471 doxorubicin and irinotecan under our experimental conditions. However, previous investigations
472 reported that this US modality significantly increased the intracellular uptake of both drugs and
473 their cytotoxic effects *in vitro* and *in vivo* [20,22,45,46]. If we consider doxorubicin first, the
474 acoustically mediated delivery of free doxorubicin (as opposed to doxorubicin loaded in MBs or
475 liposomes) enhances the membrane permeability of tumor cells to this drug, thus resulting in a
476 significant increase in its cytotoxic effects on cell suspensions or monolayers [47,48]. The *in vitro*
477 studies conducted on the tumor spheroids depicted contradictory results [15,35,49]. Indeed, Misra

478 et al. showed that this US modality increased the penetration of doxorubicin (50 μ M) inside
479 mammary tumor (MDA-MB-231) spheroids and its intracellular uptake. Surprisingly, these results
480 were not correlated with a significant inhibition of spheroid growth compared to doxorubicin
481 treatment alone. The use of a high concentration of doxorubicin, *i.e.*, 50 μ M, could explain these
482 results. Bourn et al. described a positive correlation between an increase in the intracellular uptake
483 of doxorubicin and a decrease in the viability of CRC/fibroblast (HCT-116/HFFF2) spheroids after
484 acoustically mediated delivery of doxorubicin at 3 μ M. This last study demonstrates that MB-
485 assisted US can potentiate the therapeutic efficacy of low concentrations of doxorubicin (*i.e.*, < 5
486 μ M) on spheroids, thus partly explaining our results obtained at 10 μ M doxorubicin. Indeed, we
487 failed to improve the cytotoxic effects of low concentrations of doxorubicin (< 1 μ M) on CRC
488 spheroids in the present study but also in preliminary studies (data not shown), suggesting that
489 HCT-116 cells would be highly sensitive to doxorubicin. In their study, Bourn et al. exploited CRC
490 spheroids made up of human colorectal cancer HCT-116 cells (as reported in the present study)
491 and human HFFF2 fibroblasts. It is now widely known that such coculture decreases the sensitivity
492 of tumor cells to anticancer drugs [16,49–51], thus explaining why Bourn et al. succeeded in
493 potentiating the therapeutic efficacy of low concentrations of doxorubicin on their spheroids and
494 not us. In the present study, we can only conclude that MB-assisted US did not potentiate the
495 cytotoxic effects of doxorubicin on HCT-116 spheroids. In the near future, these experiences will
496 have to be reproduced on spheroids made-up of different types of cancer cells cocultured with or
497 without other cell lines such as fibroblast, in order to conclude on the efficacy of MB-assisted US
498 to enhance the therapeutic efficacy of doxorubicin on tumor spheroids. We note that the efficacy
499 of acoustically mediated delivery of free doxorubicin has only been described in a few *in vivo*
500 tumor models [46,52,53]. Indeed, it is mainly the delivery of its liposomal formulation (Doxil[®] or

501 Caelyx[®]) as well as doxorubicin-loaded MBs, which has been reported *in vivo* due to the strong
 502 cardiotoxicity of free doxorubicin [54–56]. The use of liposomal doxorubicin will be more relevant
 503 in our further investigations on tumor spheroids.

504 **Table 1.** Description of chemotherapeutic drugs and propidium iodide.

	Molecule	Structure	Molecular weight (g/mol)	Mechanisms of action
THERAPEUTIC MOLECULES	Bleomycin		1 415.551	<ul style="list-style-type: none"> • ROS generation • Intercalation into DNA • Topoisomerase II inhibition
	Doxorubicin		543.52	<ul style="list-style-type: none"> • ROS generation • Intercalation into DNA • Topoisomerase II inhibition
	Irinotecan		586.678	Topoisomerase I inhibition
DRUG MODEL	Propidium iodide		668.403	N/A

505

506 Regarding the acoustically mediated delivery of irinotecan, several proofs of concept
 507 showed that MB-assisted US efficiently delivered free irinotecan *in vitro* [20] and *in vivo* in healthy
 508 and tumor brain tissues [20,45,57]. We demonstrated that the therapeutic efficacy of a 500 µg/mL
 509 irinotecan concentration can be achieved by delivering a 1000 times lower concentration by MB-
 510 assisted US in human glioblastoma (U-87 MG) cells [20]. *In vivo*, the acoustically mediated
 511 delivery of free irinotecan in a glioblastoma (U-87 MG) murine model resulted in a significant
 512 decrease in tumor growth compared to irinotecan treatment alone. To the best of our knowledge,
 513 spheroids have never been exploited to evaluate the acoustically mediated delivery of free
 514 irinotecan. However, they are used to assess new formulations of therapeutic MBs, in which
 515 irinotecan is loaded alone [58,59] or with other anticancer drugs [59,60]. Indeed, Gao et al.

516 demonstrated that MB-assisted US using irinotecan-loaded MBs (50 μ M) induced a significant
517 decrease in the viability of pancreatic tumor spheroids compared to irinotecan-loaded MB
518 treatment alone. As opposed to our irinotecan delivery strategy, the encapsulation of irinotecan
519 inside MBs limits its intracellular uptake and therefore its cytotoxic effects. The exposure of tumor
520 cells and irinotecan-loaded MBs to US induces the release of irinotecan from MBs and increases
521 the membrane permeability of tumor cells to this drug, thus potentiating its therapeutic efficacy.
522 Regardless of the type of tumor cells and drug delivery protocol, the loading of irinotecan inside
523 the MBs is the main reason why these authors observed a significant difference in spheroid
524 viability between their experimental and control conditions, contrary to our present study.

525 In addition to the further improvements described above, future developments would
526 consist of the use of vascularized tumor spheroid-on chip where the spheroids will be formed from
527 patient-derived cancer cells and have different sizes [61–63]. This strategy will be more relevant
528 to design and to assess protocols (*e.g.*, US parameters, MB and drug-related parameters,
529 therapeutic schemes, *etc.*) for acoustically mediated delivery of therapeutic molecules of different
530 molecular weights in a pathophysiological context close to that encountered *in vivo*.

531 CONCLUSION

532 In summary, the present results suggest that MB-assisted US enhanced the therapeutic
533 efficacy of bleomycin on CRC spheroids but not that of doxorubicin and irinotecan. Nevertheless,
534 further improvements are required to potentiate their therapeutic efficacies. The exploitation of
535 tumor spheroids should be a complementary approach to design and validate innovative protocols
536 for acoustically mediated drug delivery.

537 ACKNOWLEDGMENT

538 The authors acknowledge J.Y. Tartu (UMR 1253, iBrain, Université de Tours, Inserm,
539 Tours, France) for the design of ultrasound setup, Dr. Virginie André (Regional Center of
540 Cancerology, Henry Kaplan, CHRU de Tours, Tours, France) for providing the irinotecan and the
541 Electron Microscopy (EM) Facility (IBiSA) of Tours University ([http://microscopies.med.univ-
542 tours.fr](http://microscopies.med.univ-tours.fr)) for technical support.

543 *FUNDING SOURCES*

544 This work was supported, in part, by Inserm, Université de Tours and Ligue Contre le
545 Cancer (S.S., J.M.E.). M.R. was the recipient of a Ph.D. fellowship from the Region Centre-Val
546 de Loire.

547 *ABBREVIATIONS*

548 2D, two-dimensional; 3D, three-dimensional; CRC spheroid, colorectal cancer spheroid;
549 DPBS, Dulbecco's phosphate-buffered saline solution; FCS, fetal calf serum; MB-assisted US,
550 microbubble-assisted ultrasound; MBs, microbubbles; PI, propidium iodide; PNP, peak negative
551 pressure; PRP, pulse repetition period; SEM, mean standard deviation; TEM, transmission electron
552 microscopy; ULA, ultra-low attachment; US, ultrasound.

553 *REFERENCES*

- 554 1. Roy, M.; Alix, C.; Bouakaz, A.; Serrière, S.; Escoffre, J.-M. Tumor Spheroids as Model to
555 Design Acoustically Mediated Drug Therapies: A Review. *Pharmaceutics* **2023**, *15*, 806,
556 doi:10.3390/pharmaceutics15030806.
- 557 2. Torisawa, Y.-S.; Takagi, A.; Shiku, H.; Yasukawa, T.; Matsue, T. A Multicellular Spheroid-
558 Based Drug Sensitivity Test by Scanning Electrochemical Microscopy. *Oncol Rep* **2005**, *13*,
559 1107–1112.
- 560 3. Ward, J.P.; King, J.R. Mathematical Modelling of Drug Transport in Tumour Multicell
561 Spheroids and Monolayer Cultures. *Mathematical Biosciences* **2003**, *181*, 177–207,
562 doi:10.1016/S0025-5564(02)00148-7.
- 563 4. Curcio, E.; Salerno, S.; Barbieri, G.; De Bartolo, L.; Drioli, E.; Bader, A. Mass Transfer and
564 Metabolic Reactions in Hepatocyte Spheroids Cultured in Rotating Wall Gas-Permeable

- 565 Membrane System. *Biomaterials* **2007**, *28*, 5487–5497,
566 doi:10.1016/j.biomaterials.2007.08.033.
- 567 5. Browning, A.P.; Sharp, J.A.; Murphy, R.J.; Gunasingh, G.; Lawson, B.; Burrage, K.; Haass,
568 N.K.; Simpson, M. Quantitative Analysis of Tumour Spheroid Structure. *eLife* **10**, e73020,
569 doi:10.7554/eLife.73020.
- 570 6. Pampaloni, F.; Reynaud, E.G.; Stelzer, E.H.K. The Third Dimension Bridges the Gap
571 between Cell Culture and Live Tissue. *Nat Rev Mol Cell Biol* **2007**, *8*, 839–845,
572 doi:10.1038/nrm2236.
- 573 7. Pu, C.; Chang, S.; Sun, J.; Zhu, S.; Liu, H.; Zhu, Y.; Wang, Z.; Xu, R.X. Ultrasound-Mediated
574 Destruction of LHRHa Targeted and Paclitaxel Loaded Lipid Microbubbles for the Treatment
575 of Intraperitoneal Ovarian Cancer Xenografts. *Mol Pharm* **2014**, *11*, 49–58,
576 doi:10.1021/mp400523h.
- 577 8. Zhang, Y.; Chang, S.; Sun, J.; Zhu, S.; Pu, C.; Li, Y.; Zhu, Y.; Wang, Z.; Xu, R.X. Targeted
578 Microbubbles for Ultrasound Mediated Short Hairpin RNA Plasmid Transfection to Inhibit
579 Survivin Gene Expression and Induce Apoptosis of Ovarian Cancer A2780/DDP Cells. *Mol*
580 *Pharm* **2015**, *12*, 3137–3145, doi:10.1021/mp500835z.
- 581 9. Okunaga, S.; Takasu, A.; Meshii, N.; Imai, T.; Hamada, M.; Iwai, S.; Yura, Y. Ultrasound as
582 a Method to Enhance Antitumor Ability of Oncolytic Herpes Simplex Virus for Head and
583 Neck Cancer. *Cancer Gene Ther* **2015**, *22*, 163–168, doi:10.1038/cgt.2015.3.
- 584 10. Sun, L.; Zhang, J.; Xu, M.; Zhang, L.; Tang, Q.; Chen, J.; Gong, M.; Sun, S.; Ge, H.; Wang,
585 S.; et al. Ultrasound Microbubbles Mediated Sonosensitizer and Antibody Co-Delivery for
586 Highly Efficient Synergistic Therapy on HER2-Positive Gastric Cancer. *ACS Appl Mater*
587 *Interfaces* **2022**, *14*, 452–463, doi:10.1021/acsami.1c21924.
- 588 11. Kooiman, K.; Roovers, S.; Langeveld, S.A.G.; Kleven, R.T.; Dewitte, H.; O'Reilly, M.A.;
589 Escoffre, J.-M.; Bouakaz, A.; Verweij, M.D.; Hynynen, K.; et al. Ultrasound-Responsive
590 Cavitation Nuclei for Therapy and Drug Delivery. *Ultrasound Med Biol* **2020**, *46*, 1296–
591 1325, doi:10.1016/j.ultrasmedbio.2020.01.002.
- 592 12. Escoffre, J.-M.; Bouakaz, A. Minireview: Biophysical Mechanisms of Cell Membrane
593 Sonopermeabilization. Knowns and Unknowns. *Langmuir* **2019**, *35*, 10151–10165,
594 doi:10.1021/acs.langmuir.8b03538.
- 595 13. Lentacker, I.; De Cock, I.; Deckers, R.; De Smedt, S.C.; Moonen, C.T.W. Understanding
596 Ultrasound Induced Sonoporation: Definitions and Underlying Mechanisms. *Adv Drug Deliv*
597 *Rev* **2014**, *72*, 49–64, doi:10.1016/j.addr.2013.11.008.
- 598 14. Snipstad, S.; Vikedal, K.; Maardalen, M.; Kurbatskaya, A.; Sulheim, E.; Davies, C. de L.
599 Ultrasound and Microbubbles to Beat Barriers in Tumors: Improving Delivery of
600 Nanomedicine. *Adv Drug Deliv Rev* **2021**, *177*, 113847, doi:10.1016/j.addr.2021.113847.
- 601 15. Misra, R.; Rajic, M.; Sathiyamoorthy, K.; Karshafian, R. Ultrasound and Microbubbles
602 (USMB) Potentiated Doxorubicin Penetration and Distribution in 3D Breast Tumour
603 Spheroids. *Journal of Drug Delivery Science and Technology* **2021**, *61*, 102261,
604 doi:10.1016/j.jddst.2020.102261.
- 605 16. Roovers, S.; Deprez, J.; Priwitaningrum, D.; Lajoinie, G.; Rivron, N.; Declercq, H.; De
606 Wever, O.; Stride, E.; Le Gac, S.; Versluis, M.; et al. Sonoprinting Liposomes on Tumor
607 Spheroids by Microbubbles and Ultrasound. *J Control Release* **2019**, *316*, 79–92,
608 doi:10.1016/j.jconrel.2019.10.051.

- 609 17. Dominijanni, A.; Devarasetty, M.; Soker, S. Manipulating the Tumor Microenvironment in
610 Tumor Organoids Induces Phenotypic Changes and Chemoresistance. *iScience* **2020**, *23*,
611 101851, doi:10.1016/j.isci.2020.101851.
- 612 18. Shi, W.; Kwon, J.; Huang, Y.; Tan, J.; Uhl, C.G.; He, R.; Zhou, C.; Liu, Y. Facile Tumor
613 Spheroids Formation in Large Quantity with Controllable Size and High Uniformity. *Sci Rep*
614 **2018**, *8*, 6837, doi:10.1038/s41598-018-25203-3.
- 615 19. Griseti, E.; Kolosnjaj-Tabi, J.; Gibot, L.; Fourquaux, I.; Rols, M.-P.; Yousfi, M.; Merbahi,
616 N.; Golzio, M. Pulsed Electric Field Treatment Enhances the Cytotoxicity of Plasma-
617 Activated Liquids in a Three-Dimensional Human Colorectal Cancer Cell Model. *Sci Rep*
618 **2019**, *9*, 7583, doi:10.1038/s41598-019-44087-5.
- 619 20. Escoffre, J.-M.; Novell, A.; Serrière, S.; Lecomte, T.; Bouakaz, A. Irinotecan Delivery by
620 Microbubble-Assisted Ultrasound: In Vitro Validation and a Pilot Preclinical Study. *Mol*
621 *Pharm* **2013**, *10*, 2667–2675, doi:10.1021/mp400081b.
- 622 21. Bressand, D.; Novell, A.; Girault, A.; Raoul, W.; Fromont-Hankard, G.; Escoffre, J.-M.;
623 Lecomte, T.; Bouakaz, A. Enhancing Nab-Paclitaxel Delivery Using Microbubble-Assisted
624 Ultrasound in a Pancreatic Cancer Model. *Mol Pharm* **2019**, *16*, 3814–3822,
625 doi:10.1021/acs.molpharmaceut.9b00416.
- 626 22. Escoffre, J.M.; Piron, J.; Novell, A.; Bouakaz, A. Doxorubicin Delivery into Tumor Cells
627 with Ultrasound and Microbubbles. *Mol Pharm* **2011**, *8*, 799–806, doi:10.1021/mp100397p.
- 628 23. Escoffre, J.-M.; Novell, A.; Piron, J.; Zeghimi, A.; Doinikov, A.; Bouakaz, A. Microbubble
629 Attenuation and Destruction: Are They Involved in Sonoporation Efficiency? *IEEE*
630 *Transactions on Ultrasonics, Ferroelectrics, and Frequency Control* **2013**, *60*, 46–52,
631 doi:10.1109/TUFFC.2013.2536.
- 632 24. Wang, M.; Zhang, Y.; Cai, C.; Tu, J.; Guo, X.; Zhang, D. Sonoporation-Induced Cell
633 Membrane Permeabilization and Cytoskeleton Disassembly at Varied Acoustic and
634 Microbubble-Cell Parameters. *Sci Rep* **2018**, *8*, 3885, doi:10.1038/s41598-018-22056-8.
- 635 25. Potočnik, T.; Miklavčič, D.; Maček Lebar, A. Effect of Electroporation and Recovery
636 Medium pH on Cell Membrane Permeabilization, Cell Survival and Gene Transfer Efficiency
637 in Vitro. *Bioelectrochemistry* **2019**, *130*, 107342, doi:10.1016/j.bioelechem.2019.107342.
- 638 26. Escoffre, J.-M.; Portet, T.; Favard, C.; Teissié, J.; Dean, D.S.; Rols, M.-P. Electromediated
639 Formation of DNA Complexes with Cell Membranes and Its Consequences for Gene
640 Delivery. *Biochimica et Biophysica Acta (BBA) - Biomembranes* **2011**, *1808*, 1538–1543,
641 doi:10.1016/j.bbamem.2010.10.009.
- 642 27. Memari, E.; Hui, F.; Yusefi, H.; Helfield, B. Fluid Flow Influences Ultrasound-Assisted
643 Endothelial Membrane Permeabilization and Calcium Flux. *Journal of Controlled Release*
644 **2023**, *358*, 333–344, doi:10.1016/j.jconrel.2023.05.004.
- 645 28. Lacroix-Lamandé, S.; Bernardi, O.; Pezier, T.; Barilleau, E.; Burlaud-Gaillard, J.; Gagneux,
646 A.; Velge, P.; Wiedemann, A. Differential Salmonella Typhimurium Intracellular
647 Replication and Host Cell Responses in Caecal and Ileal Organoids Derived from Chicken.
648 *Veterinary Research* **2023**, *54*, 63, doi:10.1186/s13567-023-01189-3.
- 649 29. Meijering, B.D.M.; Henning, R.H.; Van Gilst, W.H.; Gavrilovic, I.; Van Wamel, A.;
650 Deelman, L.E. Optimization of Ultrasound and Microbubbles Targeted Gene Delivery to
651 Cultured Primary Endothelial Cells. *J Drug Target* **2007**, *15*, 664–671,
652 doi:10.1080/10611860701605088.

- 653 30. Keller, S.; Bruce, M.; Averkiou, M.A. Ultrasound Imaging of Microbubble Activity During
654 Sonoporation Pulse Sequences. *Ultrasound Med Biol* **2019**, *45*, 833–845,
655 doi:10.1016/j.ultrasmedbio.2018.11.011.
- 656 31. Eck, M.; Aronovich, R.; Ilovitsh, T. Efficacy Optimization of Low Frequency Microbubble-
657 Mediated Sonoporation as a Drug Delivery Platform to Cancer Cells. *International Journal*
658 *of Pharmaceutics: X* **2022**, *4*, 100132, doi:10.1016/j.ijpx.2022.100132.
- 659 32. Kotopoulos, S.; Popa, M.; Mayoral Safont, M.; Murvold, E.; Haugse, R.; Langer, A.;
660 Dimceviski, G.; Lam, C.; Bjånes, T.; Gilja, O.H.; et al. SonoVue® vs. Sonazoid™ vs.
661 Optison™: Which Bubble Is Best for Low-Intensity Sonoporation of Pancreatic Ductal
662 Adenocarcinoma? *Pharmaceutics* **2022**, *14*, 98, doi:10.3390/pharmaceutics14010098.
- 663 33. Wang, G.; Zhuo, Z.; Xia, H.; Zhang, Y.; He, Y.; Tan, W.; Gao, Y. Investigation into the
664 Impact of Diagnostic Ultrasound with Microbubbles on the Capillary Permeability of Rat
665 Hepatomas. *Ultrasound Med Biol* **2013**, *39*, 628–637,
666 doi:10.1016/j.ultrasmedbio.2012.11.004.
- 667 34. Pascal, A.; Li, N.; Lechtenberg, K.J.; Rosenberg, J.; Airan, R.D.; James, M.L.; Bouley, D.M.;
668 Pauly, K.B. Histologic Evaluation of Activation of Acute Inflammatory Response in a Mouse
669 Model Following Ultrasound-Mediated Blood-Brain Barrier Using Different Acoustic
670 Pressures and Microbubble Doses. *Nanotheranostics* **2020**, *4*, 210–223,
671 doi:10.7150/ntno.49898.
- 672 35. Paškevičiūtė, M.; Januškevičienė, I.; Sakalauskienė, K.; Raišutis, R.; Petrikaitė, V.
673 Evaluation of Low-Intensity Pulsed Ultrasound on Doxorubicin Delivery in 2D and 3D
674 Cancer Cell Cultures. *Sci Rep* **2020**, *10*, 16161, doi:10.1038/s41598-020-73204-y.
- 675 36. Mehier-Humbert, S.; Bettinger, T.; Yan, F.; Guy, R.H. Plasma Membrane Poration Induced
676 by Ultrasound Exposure: Implication for Drug Delivery. *J Control Release* **2005**, *104*, 213–
677 222, doi:10.1016/j.jconrel.2005.01.007.
- 678 37. Meijering, B.D.M.; Juffermans, L.J.M.; van Wamel, A.; Henning, R.H.; Zuhorn, I.S.;
679 Emmer, M.; Versteilen, A.M.G.; Paulus, W.J.; van Gilst, W.H.; Kooiman, K.; et al.
680 Ultrasound and Microbubble-Targeted Delivery of Macromolecules Is Regulated by
681 Induction of Endocytosis and Pore Formation. *Circ Res* **2009**, *104*, 679–687,
682 doi:10.1161/CIRCRESAHA.108.183806.
- 683 38. Pron, G.; Mahrouf, N.; Orłowski, S.; Tounekti, O.; Poddevin, B.; Belehradec, J.; Mir, L.M.
684 Internalisation of the Bleomycin Molecules Responsible for Bleomycin Toxicity: A
685 Receptor-Mediated Endocytosis Mechanism. *Biochem Pharmacol* **1999**, *57*, 45–56,
686 doi:10.1016/s0006-2952(98)00282-2.
- 687 39. Hirabayashi, F.; Iwanaga, K.; Okinaga, T.; Takahashi, O.; Ariyoshi, W.; Suzuki, R.; Sugii,
688 M.; Maruyama, K.; Tominaga, K.; Nishihara, T. Epidermal Growth Factor Receptor-
689 Targeted Sonoporation with Microbubbles Enhances Therapeutic Efficacy in a Squamous
690 Cell Carcinoma Model. *PLoS One* **2017**, *12*, e0185293, doi:10.1371/journal.pone.0185293.
- 691 40. Sonoda, S.; Tachibana, K.; Uchino, E.; Yamashita, T.; Sakoda, K.; Sonoda, K.-H.; Hisatomi,
692 T.; Izumi, Y.; Sakamoto, T. Inhibition of Melanoma by Ultrasound-Microbubble-Aided Drug
693 Delivery Suggests Membrane Permeabilization. *Cancer Biol Ther* **2007**, *6*, 1276–1283,
694 doi:10.4161/cbt.6.8.4485.
- 695 41. Lamanauskas, N.; Novell, A.; Escoffre, J.-M.; Venslauskas, M.; Satkauskas, S.; Bouakaz, A.
696 Bleomycin Delivery into Cancer Cells in Vitro with Ultrasound and SonoVue® or BR14®
697 Microbubbles. *J Drug Target* **2013**, *21*, 407–414, doi:10.3109/1061186X.2012.761223.

- 698 42. Lu, T.; Haemmerich, D.; Liu, H.; Seynhaeve, A.L.B.; van Rhooen, G.C.; Houtsmuller, A.B.;
699 ten Hagen, T.L.M. Externally Triggered Smart Drug Delivery System Encapsulating
700 Idarubicin Shows Superior Kinetics and Enhances Tumoral Drug Uptake and Response.
701 *Theranostics* **2021**, *11*, 5700–5712, doi:10.7150/thno.55163.
- 702 43. Gallois, L.; Fiallo, M.; Garnier-Suillerot, A. Comparison of the Interaction of Doxorubicin,
703 Daunorubicin, Idarubicin and Idarubicinol with Large Unilamellar Vesicles: Circular
704 Dichroism Study. *Biochimica et Biophysica Acta (BBA) - Biomembranes* **1998**, *1370*, 31–40,
705 doi:10.1016/S0005-2736(97)00241-1.
- 706 44. Xing, J.; Zhang, X.; Wang, Z.; Zhang, H.; Chen, P.; Zhou, G.; Sun, C.; Gu, N.; Ji, M. Novel
707 Lipophilic SN38 Prodrug Forming Stable Liposomes for Colorectal Carcinoma Therapy. *Int*
708 *J Nanomedicine* **2019**, *14*, 5201–5213, doi:10.2147/IJN.S204965.
- 709 45. Beccaria, K.; Canney, M.; Goldwirt, L.; Fernandez, C.; Piquet, J.; Perier, M.-C.; Lafon, C.;
710 Chapelon, J.-Y.; Carpentier, A. Ultrasound-Induced Opening of the Blood-Brain Barrier to
711 Enhance Temozolomide and Irinotecan Delivery: An Experimental Study in Rabbits. *J*
712 *Neurosurg* **2016**, *124*, 1602–1610, doi:10.3171/2015.4.JNS142893.
- 713 46. Kovacs, Z.; Werner, B.; Rassi, A.; Sass, J.O.; Martin-Fiori, E.; Bernasconi, M. Prolonged
714 Survival upon Ultrasound-Enhanced Doxorubicin Delivery in Two Syngenic Glioblastoma
715 Mouse Models. *J Control Release* **2014**, *187*, 74–82, doi:10.1016/j.jconrel.2014.05.033.
- 716 47. Lee, N.G.; Berry, J.L.; Lee, T.C.; Wang, A.T.; Honowitz, S.; Murphree, A.L.; Varshney, N.;
717 Hinton, D.R.; Fawzi, A.A. Sonoporation Enhances Chemotherapeutic Efficacy in
718 Retinoblastoma Cells In Vitro. *Invest Ophthalmol Vis Sci* **2011**, *52*, 3868–3873,
719 doi:10.1167/iovs.10-6501.
- 720 48. Yang, S.; Wang, P.; Wang, X.; Su, X.; Liu, Q. Activation of Microbubbles by Low-Level
721 Therapeutic Ultrasound Enhances the Antitumor Effects of Doxorubicin. *Eur Radiol* **2014**,
722 *24*, 2739–2753, doi:10.1007/s00330-014-3334-3.
- 723 49. Bourn, M.D.; Batchelor, D.V.B.; Ingram, N.; McLaughlan, J.R.; Coletta, P.L.; Evans, S.D.;
724 Peyman, S.A. High-Throughput Microfluidics for Evaluating Microbubble Enhanced
725 Delivery of Cancer Therapeutics in Spheroid Cultures. *J Control Release* **2020**, *326*, 13–24,
726 doi:10.1016/j.jconrel.2020.06.011.
- 727 50. Leenhardt, R.; Camus, M.; Mestas, J.L.; Jeljeli, M.; Abou Ali, E.; Chouzenoux, S.;
728 Bordacahar, B.; Nicco, C.; Batteux, F.; Lafon, C.; et al. Ultrasound-Induced Cavitation
729 Enhances the Efficacy of Chemotherapy in a 3D Model of Pancreatic Ductal
730 Adenocarcinoma with Its Microenvironment. *Sci Rep* **2019**, *9*, 18916, doi:10.1038/s41598-
731 019-55388-0.
- 732 51. Lee, J.-H.; Kim, S.-K.; Khawar, I.A.; Jeong, S.-Y.; Chung, S.; Kuh, H.-J. Microfluidic Co-
733 Culture of Pancreatic Tumor Spheroids with Stellate Cells as a Novel 3D Model for
734 Investigation of Stroma-Mediated Cell Motility and Drug Resistance. *Journal of*
735 *Experimental & Clinical Cancer Research* **2018**, *37*, 4, doi:10.1186/s13046-017-0654-6.
- 736 52. Park, J.H.; Lee, S.; Jeon, H.; Kim, J.H.; Kim, D.J.; Im, M.; Lee, B.C. A Novel Convex
737 Acoustic Lens-Attached Ultrasound Drug Delivery System and Its Testing in a Murine
738 Melanoma Subcutaneous Model. *Int J Pharm* **2023**, *642*, 123118,
739 doi:10.1016/j.ijpharm.2023.123118.
- 740 53. Feng, S.; Qiao, W.; Tang, J.; Yu, Y.; Gao, S.; Liu, Z.; Zhu, X. Chemotherapy Augmentation
741 Using Low-Intensity Ultrasound Combined with Microbubbles with Different Mechanical
742 Indexes in a Pancreatic Cancer Model. *Ultrasound Med Biol* **2021**, *47*, 3221–3230,
743 doi:10.1016/j.ultrasmedbio.2021.07.004.

- 744 54. Lee, J.H.; Moon, H.; Han, H.; Lee, I.J.; Kim, D.; Lee, H.J.; Ha, S.-W.; Kim, H.; Chung, J.W.
745 Antitumor Effects of Intra-Arterial Delivery of Albumin-Doxorubicin Nanoparticle
746 Conjugated Microbubbles Combined with Ultrasound-Targeted Microbubble Activation on
747 VX2 Rabbit Liver Tumors. *Cancers (Basel)* **2019**, *11*, 581, doi:10.3390/cancers11040581.
- 748 55. Yu, F.T.H.; Chen, X.; Wang, J.; Qin, B.; Villanueva, F.S. Low Intensity Ultrasound Mediated
749 Liposomal Doxorubicin Delivery Using Polymer Microbubbles. *Mol Pharm* **2016**, *13*, 55–
750 64, doi:10.1021/acs.molpharmaceut.5b00421.
- 751 56. Treat, L.H.; McDannold, N.; Zhang, Y.; Vykhodtseva, N.; Hynynen, K. Improved Anti-
752 Tumor Effect of Liposomal Doxorubicin after Targeted Blood-Brain Barrier Disruption by
753 MRI-Guided Focused Ultrasound in Rat Glioma. *Ultrasound Med Biol* **2012**, *38*, 1716–1725,
754 doi:10.1016/j.ultrasmedbio.2012.04.015.
- 755 57. McDannold, N.; Zhang, Y.; Supko, J.G.; Power, C.; Sun, T.; Vykhodtseva, N.; Golby, A.J.;
756 Reardon, D.A. Blood-Brain Barrier Disruption and Delivery of Irinotecan in a Rat Model
757 Using a Clinical Transcranial MRI-Guided Focused Ultrasound System. *Sci Rep* **2020**, *10*,
758 8766, doi:10.1038/s41598-020-65617-6.
- 759 58. Ingram, N.; McVeigh, L.E.; Abou-Saleh, R.H.; Maynard, J.; Peyman, S.A.; McLaughlan,
760 J.R.; Fairclough, M.; Marston, G.; Valleley, E.M.A.; Jimenez-Macias, J.L.; et al. Ultrasound-
761 Triggered Therapeutic Microbubbles Enhance the Efficacy of Cytotoxic Drugs by Increasing
762 Circulation and Tumor Drug Accumulation and Limiting Bioavailability and Toxicity in
763 Normal Tissues. *Theranostics* **2020**, *10*, 10973–10992, doi:10.7150/thno.49670.
- 764 59. Charalambous, A.; Mico, V.; McVeigh, L.E.; Marston, G.; Ingram, N.; Volpato, M.; Peyman,
765 S.A.; McLaughlan, J.R.; Wierzbicki, A.; Loadman, P.M.; et al. Targeted Microbubbles
766 Carrying Lipid-Oil-Nanodroplets for Ultrasound-Triggered Delivery of the Hydrophobic
767 Drug, Combretastatin A4. *Nanomedicine: Nanotechnology, Biology and Medicine* **2021**, *36*,
768 102401, doi:10.1016/j.nano.2021.102401.
- 769 60. Gao, J.; Logan, K.A.; Nesbitt, H.; Callan, B.; McKaig, T.; Taylor, M.; Love, M.; McHale,
770 A.P.; Griffith, D.M.; Callan, J.F. A Single Microbubble Formulation Carrying 5-
771 Fluorouridine, Irinotecan and Oxaliplatin to Enable FOLFIRINOX Treatment of Pancreatic
772 and Colon Cancer Using Ultrasound Targeted Microbubble Destruction. *J Control Release*
773 **2021**, *338*, 358–366, doi:10.1016/j.jconrel.2021.08.050.
- 774 61. Ahn, J.; Kim, D.-H.; Koo, D.-J.; Lim, J.; Park, T.-E.; Lee, J.; Ko, J.; Kim, S.; Kim, M.; Kang,
775 K.-S.; et al. 3D Microengineered Vascularized Tumor Spheroids for Drug Delivery and
776 Efficacy Testing. *Acta Biomaterialia* **2022**, doi:10.1016/j.actbio.2022.10.009.
- 777 62. Hu, Z.; Cao, Y.; Galan, E.A.; Hao, L.; Zhao, H.; Tang, J.; Sang, G.; Wang, H.; Xu, B.; Ma,
778 S. Vascularized Tumor Spheroid-on-a-Chip Model Verifies Synergistic Vasoprotective and
779 Chemotherapeutic Effects. *ACS Biomater. Sci. Eng.* **2022**, *8*, 1215–1225,
780 doi:10.1021/acsbiomaterials.1c01099.
- 781 63. Crystal, A.S.; Shaw, A.T.; Sequist, L.V.; Friboulet, L.; Niederst, M.J.; Lockerman, E.L.;
782 Frias, R.L.; Gainor, J.F.; Amzallag, A.; Greninger, P.; et al. Patient-Derived Models of
783 Acquired Resistance Can Identify Effective Drug Combinations for Cancer. *Science* **2014**,
784 *346*, 1480–1486, doi:10.1126/science.1254721.
- 785